Particle-resolved simulation of aerosol size, composition, mixing state, and the associated optical and cloud condensation nuclei activation properties in an evolving urban plume

Rahul A. Zaveri,[1] James C. Barnard,[1] Richard C. Easter,[1] Nicole Riemer,[2] and Matthew West[3]

Received 25 November 2009; revised 3 April 2010; accepted 12 April 2010; published 11 September 2010.

[1] The recently developed particle-resolved aerosol box model PartMC-MOSAIC (Particle Monte Carlo model–Model for Simulating Aerosol Interactions and Chemistry) was used to rigorously simulate the evolution of aerosol mixing state and the associated optical and cloud condensation nuclei (CCN) activation properties in an idealized urban plume. The model explicitly resolved the size and composition of individual particles from a number of sources and tracked their evolution due to condensation, evaporation, coagulation, emission, and dilution. The ensemble black carbon (BC)–specific absorption cross section increased by 40% over the course of 2 days due to BC aging by condensation and coagulation. Threefold and fourfold enhancements in CCN/CN ratios were predicted to occur within 6 h for 0.2% and 0.5% supersaturations (S), respectively. The particle-resolved results were used to evaluate the errors in the optical and CCN activation properties that would be predicted by a conventional sectional framework that assumes monodisperse, internally mixed particles within each bin. This assumption artificially increased the ensemble BC-specific absorption by 14–30% and decreased the single scattering albedo (SSA) by 0.03–0.07, while the bin resolution had a negligible effect. In contrast, the errors in CCN/CN ratios were sensitive to the bin resolution for a chosen supersaturation. For S = 0.2%, the CCN/CN ratio predicted using 100 internally mixed bins was up to 25% higher than the particle-resolved results, while it was up to 125% higher using 10 internally mixed bins. Neglecting coagulation overpredicted aerosol water content and number concentrations (<0.2 μm), causing errors in SSA from −0.02 to 0.035 and overprediction of CCN concentrations by 25–80% at S = 0.5%.

Citation: Zaveri, R. A., J. C. Barnard, R. C. Easter, N. Riemer, and M. West (2010), Particle-resolved simulation of aerosol size, composition, mixing state, and the associated optical and cloud condensation nuclei activation properties in an evolving urban plume, *J. Geophys. Res.*, *115*, D17210, doi:10.1029/2009JD013616.

1. Introduction

[2] Uncertainties in the direct and indirect radiative forcings by anthropogenic aerosols estimated by the current generation of global climate models greatly exceeds that of all other forcing mechanisms combined [*Houghton et al.*, 2001; *Forster et al.*, 2007]. Among other key advances, the next generation of climate models requires improved physical and chemical properties of both anthropogenic and natural aerosols, including their number concentration, particle size and size-dependent composition and mixing state, optical properties, solubility, and the ability to serve as nuclei of cloud particles [*Ghan and Schwartz*, 2007].

[3] Anthropogenic and natural aerosol particles range from a few nanometers to a few microns in size and can be composed of a wide variety of primary and secondary species. Primary species are those that are directly emitted into the atmosphere such as soot from fossil fuel combustion, industrial particles, cooking particles, sea salt, dust, biomass burning particles, etc. Secondary species are various low-volatile and semivolatile gas phase oxidation products or direct emissions such as sulfuric acid, nitric acid, ammonia, and myriad low-volatile and semivolatile organic compounds that can partition into the particle phase. Secondary aerosol particles can also form via homogeneous nucleation of low volatility gases such as sulfuric acid and large molecular weight oxidized organic species.

[1] Atmospheric Sciences and Global Change Division, Pacific Northwest National Laboratory, Richland, Washington, USA.
[2] Department of Atmospheric Sciences, University of Illinois at Urbana-Champaign, Urbana, Illinois, USA.
[3] Department of Mechanical Science and Engineering, University of Illinois at Urbana-Champaign, Urbana, Illinois, USA.

0148-0227/10/2009JD013616

[4] Primary particles and particles formed via homogeneous nucleation are initially "externally mixed" (i.e., each type of primary aerosol has a distinct size distribution and composition). Upon interacting with semivolatile gases in the atmosphere via condensation (and evaporation) and with other particles of different compositions via coagulation, these particles undergo changes in size and chemical composition and gradually become "internally mixed" to varying degrees. This process of evolution of aerosol size, composition, and mixing state is referred to as "aging" of aerosols. Evidence from laboratory, field measurements, and modeling studies shows that optical properties [*Jacobson*, 2001; *Schnaiter et al.*, 2003; *Kleinman et al.*, 2007] and cloud condensation nuclei activation properties [*Cantrell et al.*, 2001; *Mochida et al.*, 2006; *Kuwata et al.*, 2007; *Medina et al.*, 2007; *Cubison et al.*, 2008; *Furutani et al.*, 2008] are strongly dependent on aerosol size, composition, and mixing state.

[5] Accurately simulating evolution of aerosol size, composition, and mixing state and the associated optical and cloud condensation nuclei (CCN) activation properties in a mixture of different types of primary and secondary aerosols is a numerically difficult and computationally expensive problem. Sources of uncertainties and errors in predicting these quantities include (1) incomplete understanding of the various processes and knowledge gaps in the fundamental properties of aerosols and (2) various assumptions and numerical simplifications that are typically made in aerosol models for computational efficiency. In this paper, we focus our attention on the effects of assumptions and simplifications made in the representation of aerosol mixing state. From a computational standpoint, if an aerosol particle can contain varying fractions of N chemical components (e.g., $N = 10$ with sulfate, nitrate, chloride, carbonate, ammonium, sodium, calcium, primary organics, secondary organics, black carbon), then the mixing state is an N-dimensional space and the size-resolved particle composition distribution is a multivariate function. Thus, ideally an N-dimensional fixed grid sectional model is required to accurately resolve composition of any type of particle that can form due to condensation and heterocoagulation. A sectional model consisting of, say, 10 size sections (which is fairly coarse) then translates into 10^N grid points in the size and species mass dimensions. However, many comprehensive sectional aerosol modules have typically considered only one particle size distribution spread over discrete size bins [e.g., *Capaldo et al.*, 2000; *Zhang et al.*, 2004; *Zaveri et al.*, 2008a]. Species within a given bin are assumed to be internally mixed, while different bins are treated as externally mixed. This assumption artificially ages freshly emitted particles instantly and thereby distorts the theoretical understanding of the life cycles of different types of aerosols as well as their optical and CCN activation properties. In some sectional models, two or more distributions have been used to transfer externally mixed aerosols to various internal mixtures [*Jacobson et al.*, 1994; *Fassi-Fihri et al.*, 1997; *Kleeman et al.*, 1997; *Russell and Seinfeld*, 1998].

[6] Many modal aerosol modules used in global models have also typically implemented a minimal treatment of mixing state using separate modes for freshly emitted hydrophobic particles and for aged hygroscopic particles [e.g., *Wilson et al.*, 2001; *Stier et al.*, 2005]. *Jacobson* [2001, 2002] formulated a framework for a generalized sectional model consisting of any number of size distributions, size bins in each distribution, and components in each distribution and first performed global simulations of aerosol mixing state using 18 size distributions, with 17 size bins per distribution. Transfer of particles across bins due to condensation and coagulation was calculated with the moving center approach of *Jacobson* [1997]. Subsequently, *Jacobson* [2003] also developed numerical techniques for cloud and precipitation development from multiple aerosol size distributions. Recently, *Bauer et al.* [2008] developed a treatment of mixing state that used a two-moment representation of the 16 modes of different types. Also, *Oshima et al.* [2009] applied a mixing-state resolved version of the MADRID (Model of Aerosol Dynamics, Reaction, Ionization, and Dissolution) sectional box model [*Zhang et al.*, 2004] to evaluate the effects of aerosol mixing state on optical and CCN activation properties. Their model used a two-dimensional aerosol representation of 40 size sections ranging from 0.0215 to 10 μm, with black carbon (BC) mass fractions divided into 10 even sections between 0% and 100%. Coagulation was ignored, and the transfer of particles across the two-dimensional bins due to condensation was calculated with the moving center approach of *Jacobson* [1997]. While considerable progress has been made in this area, a rigorous simulation of the evolution of aerosol mixing state and its influence on optical and CCN activation properties has not been done.

[7] A computationally efficient approach that can accurately represent important aspects of the aerosol mixing state is ultimately needed for use in global models. A model that rigorously resolves and simulates the full aerosol mixing state (one that is free of the artificial mixing of composition and numerical diffusion in sectional and modal models) is also necessary to evaluate and improve simpler and more efficient approaches. To this end, we recently developed a particle-resolved aerosol box model by coupling the comprehensive aerosol chemistry model MOSAIC (Model for Simulating Aerosol Interactions and Chemistry) [*Zaveri et al.* 2008a] with the stochastic aerosol coagulation module Particle Monte Carlo model (PartMC) [*Riemer et al.*, 2009]. The coupled Lagrangian box model, referred to as PartMC-MOSAIC, was applied to study the evolution of soot mixing state due to coagulation and condensation in an idealized urban plume in the work of *Riemer et al.* [2009]. In a subsequent study, *Riemer et al.* [2010] investigated the aging of black carbon–containing particles with respect to CCN activation and showed that, depending on the supersaturation threshold, the aging time scales can vary between 0.06 and 10 h during the day and between 6 and 54 h during the night for the chosen urban plume scenario.

[8] Here we apply PartMC-MOSAIC to investigate the influence of aerosol mixing state evolution on optical and CCN activation properties in an urban plume and evaluate errors and biases introduced in these properties in a traditional sectional framework due to (1) internal mixture assumption, (2) bin size resolution, and (3) ignoring coagulation.

2. Model Description and Application

2.1. PartMC-MOSAIC

[9] The main features of the PartMC-MOSAIC model are briefly described here; a detailed description is given in the

work of *Riemer et al.* [2009]. PartMC explicitly resolves and tracks the composition of many individual aerosol particles (about 10^5) within a well-mixed computational volume V_{box} (few cm^3) that represents a much larger, well-mixed air parcel of interest. The relative particle positions within this computational volume are not tracked. Emission of primary aerosol particles into the computational volume, vertical entrainment and dilution with background air, and Brownian coagulation processes are simulated stochastically in PartMC.

[10] PartMC is coupled with the state-of-the-art aerosol chemistry model MOSAIC, which is described in detail in the work of *Zaveri et al.* [2008a]. MOSAIC includes deterministic treatments for gas phase photochemistry [*Zaveri and Peters*, 1999], particle phase thermodynamics [*Zaveri et al.*, 2005a, 2005b], and fully dynamic (kinetic) gas-particle mass transfer [*Zaveri et al.*, 2008a]. The standalone MOSAIC box model also includes nucleation based on the work of *Wexler et al.* [1994], but it is presently not implemented in PartMC-MOSAIC. MOSAIC treats key aerosol species including sulfate (SO_4), nitrate (NO_3), chloride (Cl), carbonate (CO_3), methanesulfonic acid (MSA), ammonium (NH_4), sodium (Na), calcium (Ca), other inorganic mass (OIN), BC, primary organic aerosol (POA), and secondary organic aerosol (SOA). OIN includes species such as SiO_2, metal oxides, and other unmeasured or unknown inorganic species present in aerosols. All particles are assumed to be spherical. The version of the MOSAIC box model used here includes a fully dynamic gas-particle mass transfer treatment for SOA (as opposed to bulk equilibrium) based on the SORGAM scheme [*Schell et al.*, 2001]. The original SORGAM scheme produced much lower SOA levels compared to ambient levels typically observed in urban environments [*Volkamer et al.*, 2006; *Kleinman et al.*, 2007]. For the purpose of this study, we modified some of the SORGAM model parameters (increased gas phase yields by a factor of 2 and reduced saturation vapor pressures by a factor of 2) so that it artificially increased SOA production to give overall SOA concentrations that are comparable to observations.

[11] The coupled model system PartMC-MOSAIC predicts number, mass, and full composition distributions on a particle-by-particle basis. This approach allows particles of same size to have different compositions and therefore different optical and CCN activation properties as well. Simulating all particles explicitly in a population of different types of aerosol completely eliminates errors caused by numerical diffusion and artificial internal mixing, which are inherently present in sectional and modal models. Thus, PartMC-MOSAIC can be used as a numerical benchmark for evaluating sectional and modal aerosol models. The optical and CCN activation properties modules implemented in the PartMC-MOSAIC model are described below.

2.2. Optical Properties Module

[12] Atmospheric radiative transfer models require as input aerosol optical properties defined for a small volume containing many aerosol particles. These properties are the ensemble extinction, scattering, and absorption coefficients ($B_{ext}(\lambda)$, $B_{scat}(\lambda)$, and $B_{abs}(\lambda)$ (Mm^{-1}), respectively); the ensemble single scattering albedo (SSA); and the ensemble asymmetry parameter g; all of which are functions of wet particle size and chemical composition distributions at a given wavelength λ. In the PartMC-MOSAIC framework, determining these parameters is a two-step procedure. In the first step, we determine the optical properties of each particle within the computational volume, and in the second step, we sum or average these properties over all the particles in the computational volume to determine the ensemble aerosol radiative parameters [*Lacis and Mishchenko*, 1995].

[13] The calculation of optical properties of each particle is done using conventional Mie theory, which assumes the particle to be spherical. The substances composing each particle are assumed to be well mixed within a particle, with the exception of BC. When BC is not present in a particle, the refractive indices of each substance are volume averaged [*Lesins et al.*, 2002] to give a single (complex) refractive index for the particle, which is needed as input to the Mie algorithm. However, when a strong absorber such as BC is present, volume averaging over all constituents, including BC, tends to overestimate the absorption [*Bond et al.*, 2006]. Here we adopt the shell-and-core configuration [*Ackerman and Toon*, 1981] in which BC forms the core of the particle and the other nonabsorbing substances, when present, compose the shell. This configuration, while still approximate, appears to simulate enhancement in soot absorption reasonably well [*Fuller et al.*, 1999; *Schnaiter et al.*, 2003; *Saathoff et al.*, 2003]. The shell-and-core assumption holds up well even when the BC core is randomly distributed inside a particle provided that the core occupies a relatively large volume fraction of the aerosol [*Fuller et al.*, 1999].

[14] Thus, in the first step, the optical properties module determines the shell and core refractive indices for each particle i as described above and passes them along with wet particle diameter to the Mie code to calculate the scattering cross section $\sigma'_{scat,i}(\lambda)$ (m^2), extinction cross section $\sigma'_{ext,i}(\lambda)$ (m^2), absorption cross section $\sigma'_{abs,i}(\lambda) = \sigma'_{ext,i}(\lambda) - \sigma'_{scat,i}(\lambda)$ (m^2), and the asymmetry parameter for scattering $g'_i(\lambda)$. The prime in the symbols for these variables denote that they are per particle quantities as opposed to ensemble aerosol quantities. Additionally, the black carbon–specific absorption $SA'_i(\lambda)$ ($m^2\ g^{-1}$) and specific scattering $SS'_i(\lambda)$ ($m^2\ g^{-1}$) for each particle are calculated as

$$SA'_i(\lambda) = \frac{\sigma'_{abs,i}(\lambda)}{M_{BC,i}} \text{ and} \tag{1}$$

$$SS'_i(\lambda) = \frac{\sigma'_{scat,i}(\lambda)}{M_{aer,i}}, \tag{2}$$

where $M_{BC,i}$ is the mass of BC in particle i (for BC containing particles only) and $M_{aer,i}$ is the total mass (including water) of particle i.

[15] In the second step, the particle quantities are summed or averaged to determine the ensemble aerosol optical properties. The ensemble scattering, absorption, and extinction coefficients are merely the sum of their respective cross sections divided by the computational volume (V_{box}) that contains the particles,

$$B_{scat}(\lambda) = \frac{\sum_{i=1}^{N} \sigma'_{scat,i}(\lambda)}{V_{box}} \tag{3}$$

Table 1. List of Refractive Indices and Hygroscopicity Values for Model Species

Species	Refractive Index at λ = 550 nm	Hygroscopicity, κ
H_2SO_4	1.5–0*i*	0.9
$(NH_4)_2SO_4$	1.5–0*i*	0.61
$(NH_4)_3H(SO_4)_2$	1.5–0*i*	0.65
NH_4HSO_4	1.5–0*i*	0.61
NH_4NO_3	1.5–0*i*	0.67
H_2O	1.33–0*i*	–
POA	1.45–0*i*	0.001
SOA species	1.45–0*i*	0.1
BC	1.82–0.74*i*	0.001

$$B_{\text{ext}}(\lambda) = \frac{\sum_{i=1}^{N} \sigma'_{\text{ext},i}(\lambda)}{V_{\text{box}}}, \text{and} \tag{4}$$

$$B_{\text{abs}}(\lambda) = B_{\text{ext}}(\lambda) - B_{\text{scat}}(\lambda), \tag{5}$$

where N is the total number of particles in the computational volume. The ensemble single scattering albedo is calculated as

$$\text{SSA}(\lambda) = B_{\text{scat}}(\lambda)/B_{\text{ext}}(\lambda), \tag{6}$$

and the ensemble asymmetry parameter for scattering is calculated as

$$g(\lambda) = \sum_{i=1}^{N} \sigma'_{\text{scat},i}(\lambda) g'_i(\lambda) \Bigg/ \sum_{i=1}^{N} \sigma'_{\text{scat},i}(\lambda). \tag{7}$$

Finally, the ensemble black carbon–specific absorption SA (λ) ($m^2\ g^{-1}$) and ensemble specific scattering SS(λ) ($m^2\ g^{-1}$) are calculated as

$$\text{SA}(\lambda) = \frac{\sum_{i=1}^{N} \sigma'_{\text{abs},i}(\lambda)}{\sum_{i=1}^{N} M_{\text{BC},i}} \text{and} \tag{8}$$

$$\text{SS}(\lambda) = \frac{\sum_{i=1}^{N} \sigma'_{\text{scat},i}(\lambda)}{\sum_{i=1}^{N} M_{\text{aer},i}}. \tag{9}$$

The complex refractive index values (at λ = 550 nm) assigned to individual aerosol components used in this study are listed in Table 1. In this table, both the real and imaginary parts of the refractive index for BC are the midpoints of plausible ranges for these quantities as given in the work of *Bond and Bergstrom* [2006].

2.3. CCN Activation Properties Module

[16] Since PartMC-MOSAIC explicitly simulates and tracks the dry size and composition of each individual particle in a population of aerosol of different types, we can calculate the critical supersaturation (S_c) that each particle would need to activate to become a cloud drop. The equilibrium saturation ratio (S) over an aqueous particle i is given by the Köhler equation,

$$S_i = a_{\text{w},i} \exp\left(\frac{4\sigma_{\text{sol}} M_{\text{w}}}{RT\rho_{\text{w}} D_{\text{p,wet},i}}\right), \tag{10}$$

where a_{w} is the activity of water in aqueous particle, σ_{sol} (dyne cm^{-1}) is the surface tension of the aqueous solution-air interface, M_{w} (g mol^{-1}) is the molecular weight of water, ρ_{w} (g cm^{-3}) is the density of water, R is the universal gas constant, T (K) is the temperature, and $D_{\text{p,wet}}$ (cm) is the wet diameter of the aqueous particle. We use the concept of a single, dimensionless hygroscopicity parameter to relate particle dry diameter to CCN activity [*Ghan et al.*, 2001; *Petters and Kreidenweis*, 2007]. Following the notation in the work of *Petters and Kreidenweis* [2007], the overall hygroscopicity parameter (κ) relates the dry particle volume (V_{dry}) and liquid water volume (V_{w}) in particle i to its water activity via

$$\frac{1}{a_{\text{w},i}} = 1 + \kappa_i \frac{V_{\text{dry},i}}{V_{\text{w},i}}. \tag{11}$$

Combining equations (10) and (11) and relating the dry and wet volumes to their respective diameters, we obtain the κ-Köhler equation [*Petters and Kreidenweis*, 2007],

$$S_i(D_{\text{p,wet},i}) = \frac{D^3_{\text{p,wet},i} - D^3_{\text{p,dry},i}}{D^3_{\text{p,wet},i} - D^3_{\text{p,dry},i}(1-\kappa_i)} \exp\left(\frac{4\sigma_{\text{sol}} M_{\text{w}}}{RT\rho_{\text{w}} D_{\text{p,wet},i}}\right). \tag{12}$$

Since each particle i is made up of several components j, the overall hygroscopicity κ_i is calculated using the Zdanovskii-Stokes-Robinson (ZSR) mixing rule as the sum of individual component hygroscopicities $\kappa_{i,j}$ weighted by the individual component volume fractions $\varepsilon_{i,j}$,

$$\kappa_i = \sum_j \varepsilon_{i,j} \kappa_{i,j}, \tag{13}$$

where $\varepsilon_{i,j} = V_{i,j}/V_{\text{dry},i}$, j = BC, POA, SOA, and different electrolytes (except water), assuming complete deliquescence. Electrolyte concentrations are calculated using the algorithms given in *Zaveri et al.* [2005a]. The hygroscopicity values for individual components are also listed in Table 1. Equation (12) is generally applicable over the entire range of relative humidity and solution hygroscopicity, but the use of κ values in PartMC-MOSAIC is restricted to the supersaturated ($S \geq 1$) regime to predict the conditions for cloud droplet activation. In the subsaturated ($S < 1$) regime, the aerosol thermodynamics module in MOSAIC employs the relatively more accurate a_{w}-dependent polynomials for molality for individual electrolytes along with solid-liquid equilibrium constraints to calculate water content with the ZSR mixing rule [*Zaveri et al.*, 2005a, 2005b].

[17] The critical supersaturation for a given dry particle diameter with an overall hygroscopicity κ corresponds to the maximum supersaturation value predicted by the κ-Kohler equation (12), and the corresponding wet particle diameter is referred to as the critical diameter. The critical supersaturation is thus calculated by setting the derivative of equation (12) with respect to $D_{\text{p,wet},i}$ to zero and numerically solving it

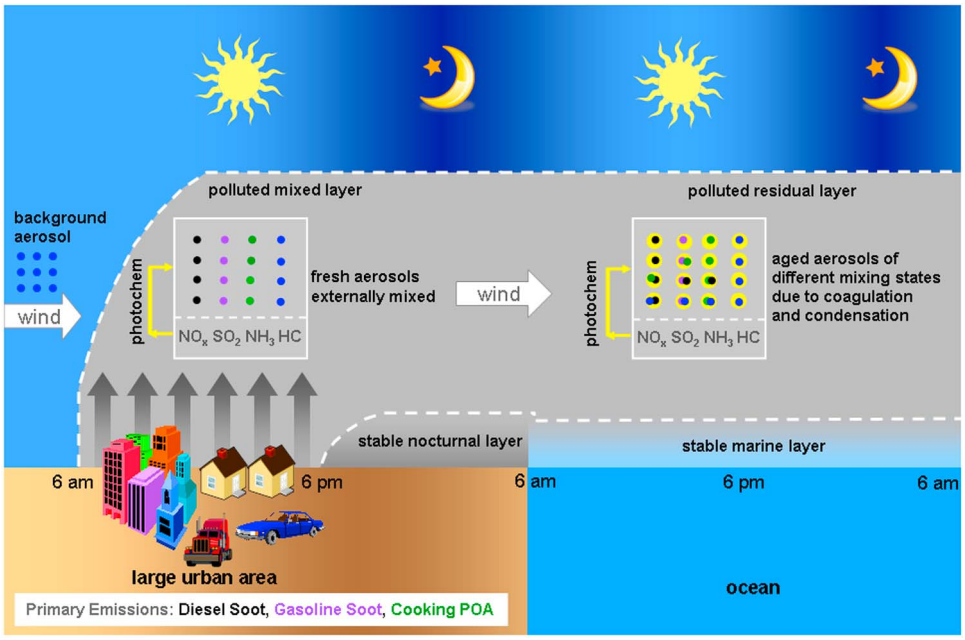

Figure 1. Schematic of the idealized urban plume scenario.

for critical wet diameter, which is substituted back in equation (12) to obtain S_c.

2.4. Idealized Urban Plume Scenario

[18] In the previous study, we applied PartMC-MOSAIC in a Lagrangian box model framework to an idealized urban plume scenario to study the evolution of aerosol mixing state due to coagulation and condensation [*Riemer et al.*, 2009]. In this study, we investigate the influence of aerosol mixing state on optical and CCN activation properties as aerosols of different types age in an evolving urban plume over a period of 2 days. Figure 1 shows the schematic of the idealized urban plume scenario, which is set up for summertime, cloud-free conditions. The urban plume scenario used here is similar to the one described in the work of *Riemer et al.* [2009], although some minor modifications and adjustments were made in this study. As in the previous study, an air parcel containing background air is advected within the mixed layer over a large urban area for a period of 12 h from 0600 to 1800 local standard time (LST). The background air is assumed to be composed of 50 ppbv O_3 and low levels of other trace gases along with an internally mixed ammonium sulfate + secondary organic aerosol with trace amounts of black carbon such that the single scattering albedo was about 0.97, a value typical for rural, relatively unpolluted areas [*Delene and Ogren*, 2002; *Dubovik et al.*, 2002].

[19] As the air parcel is advected over the large urban area, it experiences continuous emissions of NO_x, SO_2, CO, volatile organic compounds (VOCs), and primary aerosol particles of three different types: diesel soot (70% BC + 30% POA), gasoline soot (20% BC + 80% POA), and meat cooking primary organic aerosol (100% POA). The initial and background gas phase concentrations and emission rates were the same as those used in the Riemer *et al.* study, except for the NO_x emission rates, which were reduced by 50%. The size distributions for initial and background aerosols were same as those used in Riemer at al., but their concentrations were reduced by 46%. The compositions, size distributions, and emission rates of the different primary aerosols were the same as those used in the Riemer *et al.* study and are summarized here in Table 2.

[20] The air parcel also experiences dilution due to vertical entrainment of background air during the first 6 h as the mixed layer continues to grow. In the afternoon, the air parcel is advected in the fully grown mixed layer over the urban area for another 6 h. In addition and at all times, the air parcel experiences dilution with background air due to

Table 2. Initial/Background Concentrations and Emissions of Different Types of Aerosol Particles

Initial/Background	N (cm^{-3})	D_{pgN} (μm)	σ_g	Composition by Mass
Aitken mode	1800	0.02	1.45	49.6% $(NH_4)_2SO_4$ + 49.6% SOA + 0.8% BC
Accumulation mode	1500	0.116	1.65	49.6% $(NH_4)_2SO_4$ + 49.6% SOA + 0.8% BC

Emissions	E (m^{-2} s^{-1})	D_{pgN} (μm)	σ_g	Composition by Mass
Meat cooking	9×10^6	0.086	1.91	100% POA
Diesel vehicles	1.6×10^8	0.05	1.74	30% POA + 70% BC
Gasoline vehicles	5×10^7	0.05	1.74	80% POA + 20% BC

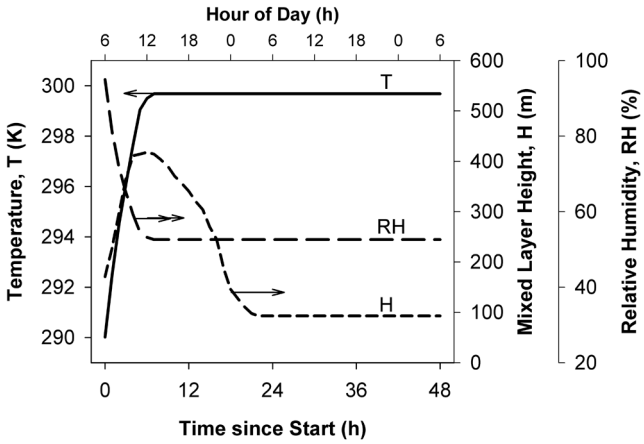

Figure 2. Prescribed meteorological variables in the urban air parcel as it is advected downwind for a period of 2 days.

horizontal dispersion, which is modeled as a first-order process, assuming a rate of 5.4% h^{-1}. In the Riemer *et al.* study, we focused on evolution of the polluted air parcel within the nocturnal stable layer after leaving the urban area at 1800 LST, and the simulation ended the next morning at 0600 LST. In the present study, we focus on the polluted air parcel that remains in the nocturnal residual layer that is decoupled from the stable surface layer. By next morning (around 0600 LST), the polluted air parcel is assumed to be over ocean, again decoupled from the stable marine surface layer, and is advected in the residual layer for another day as it continues to dilute with the background air due to horizontal dispersion [e.g., *Zaveri et al.*, 2008b].

[21] Figure 2 shows the prescribed mixed layer height along with temperature and relative humidity (RH) variations in the air parcel of interest for the 2 day simulation period. Note that temperature and RH are assumed to stay constant after the first 6 h as the air parcel of interest remains in the fully mature mixed layer or the residual layer thereafter. The assumptions of steady temperature and RH after first 6 h and constant dilution rate for the entire simulation period are made to keep the idealized scenario as simple as possible so that we can focus our analysis on the effects of coagulation and condensation processes on the evolution of optical and CCN activation properties.

[22] As mentioned earlier, the computational volume V_{box} represents the larger, well-mixed air parcel of interest in a Lagrangian framework. The initial aerosol number concentration of 3300 cm^{-3} was explicitly resolved using 100,000 particles, which corresponds to initial V_{box} of 30 cm^{-3}. The number of individual particles varied between 50,000 and 200,000 as the particle number concentration changed during the course of the 2 day simulation due to emissions, dilution, and coagulation. The variation in the number of particles and their concentrations corresponded to a variation of V_{box} between 8 and 30 cm^3.

2.5. Binning

[23] The particle-by-particle size and composition predicted by PartMC-MOSAIC were stored every hour for the 48 h simulation. The particle-resolved output was then used to compute the optical and CCN activation properties of individual particles as well as ensemble properties using the modules described above. The particle-resolved output was also processed to quantify the effects of "binning" and bin resolution on the ensemble aerosol optical properties and CCN spectra. Individual particles were binned to 100 and 10 logarithmically spaced internally mixed bins. The bins were defined in terms of dry diameter, with the lower boundary of the first bin at 0.004 μm and the upper boundary of the last bin at 2 μm. After binning, the optical and CCN properties were calculated by assuming that the particles in each bin were completely internally mixed and identical (monodisperse) in size, with $D_{p,dry}$ equal to the volume mean $D_{p,dry}$ of the bin. This approach is consistent with the moving center sectional method [*Jacobson*, 1997]. Binning to 100 bins produces an internal mixture of particles at each dry size but maintains high size resolution. With 10 bins, the size resolution is much lower, as the bin boundary changes by a factor of 1.86 between bins.

3. Results and Discussion

[24] While both condensation and coagulation affect the aerosol size and composition distributions, their effects are felt in very different ways. Condensation and evaporation change the total aerosol mass but not the total number concentration. On the other hand, coagulation reduces the number concentration while keeping the total mass concentration constant. However, coagulation of two particles may also indirectly affect the mass of semivolatile species such as NH_4NO_3, SOA, and the associated liquid water due to changes in the resulting particle's composition and phase state (i.e., solid, liquid, or mixed phase). Also, when a metastable (liquid) particle coagulates with a stable dry particle (solid), the resultant particle is assumed to take the thermodynamically stable phase state as dictated by the new composition, ambient RH, and temperature. To examine the effect of coagulation on the evolution of optical properties, we performed two simulations, with coagulation and without coagulation.

3.1. Evolution of Gas and Aerosol Composition

[25] Figure 3 shows the evolution of key trace gases mixing ratios and bulk aerosol species concentrations (i.e., summed over all particles, with and without coagulation) in the urban plume as it is advected for 2 days. Primary trace gases such as SO_2, NH_3, and NO_2 and aerosol species such as BC and POA are emitted only during the first 12 h of the simulation and thus display a maximum around 1800 LST. Their concentrations steadily declined thereafter due to chemical reaction (e.g., oxidation of SO_2 and NO_2) and dilution with background air. On the other hand, secondary trace gases such as nitric acid (HNO_3) and O_3 and secondary aerosol species such as sulfate and SOA showed two maxima and slower decay due to competition between photochemical production on each day and continued dilution with background. In contrast, secondary ammonium nitrate aerosol displayed a peculiar behavior because it is semivolatile. It formed quite rapidly when both HNO_3 and NH_3 mixing ratios were high, but later almost completely evaporated as both HNO_3 and NH_3 mixing ratios decreased due to dilution with background air. Aerosol liquid water was high at the beginning of the simulation when RH was around 90%. However, as the RH decreased with increasing

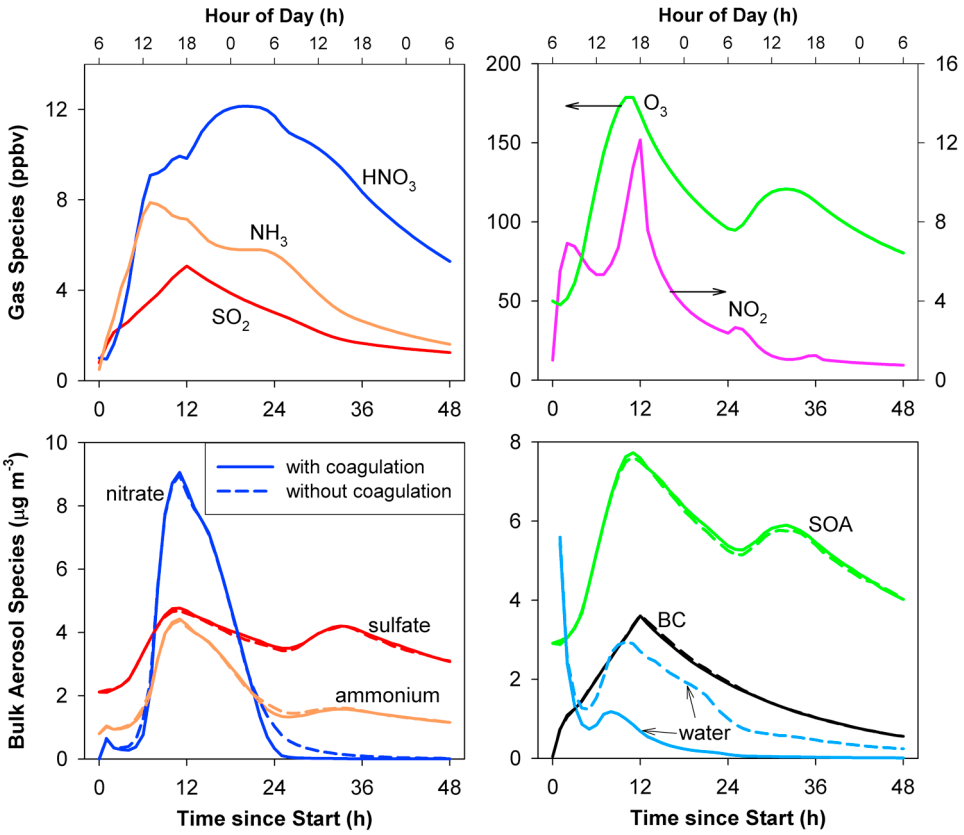

Figure 3. Evolution of key trace gas and bulk aerosol species in the urban air parcel as it is advected downwind over a period of 2 days.

temperature, the aerosol liquid water also decreased. The particles that were completely deliquesced before RH dropped below ~60% were assumed to remain supersaturated in a metastable state, while those that were emitted later were dry and remained dry for the rest of the simulation. Note that aerosol species concentrations were generally slightly higher in the simulation without coagulation than with coagulation. Small differences in mass concentrations between the two simulations are expected due to the stochastic treatments for emission and dilution. However, the more appreciable differences seen in nitrate, ammonium, and liquid water were caused by changes in the phase state when metastable (supersaturated) particles coagulated with dry solid particles.

[26] Figure 4 summarizes the evolution of the aerosol number, total mass, and BC mass size distributions for both the simulations, with and without coagulation. The changes in these size distributions reflect the combined effects of emissions, condensation, evaporation, coagulation (when present), and dilution. The initial bimodal number size distribution becomes nearly monomodal as the Aitken mode rapidly grows and merges with the accumulation mode. However, the bimodal number size distribution shape reappears later as the plume dilutes with the background aerosol. The total mass and BC size distributions display the corresponding rise due to emission or production and fall due to dilution. The BC mode geometric mean diameter also increases due to condensational growth, and the width of the mode decreases with time. Coagulation reduced the total number concentrations after 6, 12, 24, and 48 h by 15%, 25%, 50%, and 52%, respectively. Also note that the largest impact on the number concentration distribution was felt for particles smaller than 0.2 μm.

[27] We now examine the evolution of mixing states of different types of aerosol particles as a function of time. Since a given particle can be composed of several components in varying proportions, aerosol mixing state becomes a multidimensional quantity. As such we are primarily interested in the effects of aerosol mixing state on optical (especially BC-specific absorption and SSA) and CCN activation properties, which are in turn functions of BC mass fraction and hygroscopicity, respectively. It is therefore useful to visualize the evolution of aerosol mixing states of individual particles by plotting their BC dry mass fractions versus dry diameters and coloring the points by its hygroscopicity (κ) values as shown in Figure 5.

[28] Since the initial aerosol is assumed to be composed of internally mixed ammonium sulfate and secondary organic aerosol with trace amounts of black carbon, all particles have the same overall hygroscopicity and negligibly small BC mass fraction. However, as soon as fresh diesel and gasoline soot and meat cooking POA are emitted and subsequently aged due to condensation and coagulation, particles of similar dry sizes but with wide-ranging BC mass fractions and hygroscopicity values begin to appear in these plots. Also note that while freshly emitted diesel soot, gasoline soot, and cooking POA have different BC mass fractions, they are all assumed to be hydrophobic (κ = 0.001).

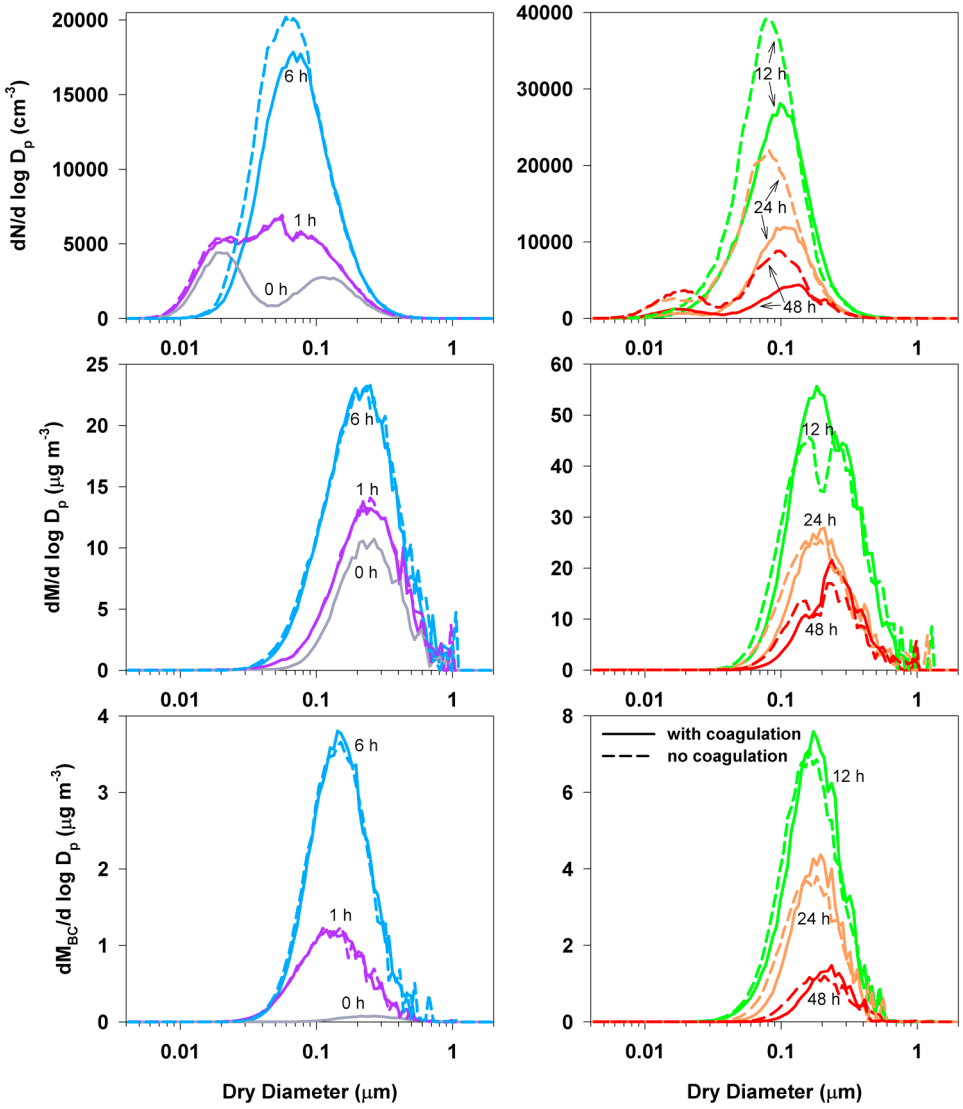

Figure 4. Evolution of (top row) number, (middle row) total dry mass, and (bottom row) BC mass size distributions for increasing times since start: (left) 0, 1, and 6 h and (right) 12, 24, and 48 h. Solid lines represent results with coagulation turned on, while dashed lines represent results without coagulation.

Thus, BC mass fraction alone is not enough to serve as a surrogate for the overall hygroscopicity of a given particle. Once the fresh emissions stopped after the first 12 h, the existing urban aerosols in the plume continued to age due to condensation and coagulation. As a result, their BC mass fractions gradually decreased, while their hygroscopicity values increased. However, even after 2 days of processing, the BC dry mass fraction still varied between 0 and 0.4 and the κ values varied between about 0.1 and 0.6.

3.2. Evolution of Optical Properties

3.2.1. Particle-Resolved Results

[29] Figure 6 shows the time evolution of BC-specific absorption cross section (SA′) of 550 nm radiation by individual aerosol particles as a function of their wet diameter. Each point in these plots represents an individual particle and is colored by its BC dry mass fraction. The BC-specific absorption cross sections of particles less than about 0.07 μm wet diameter are ~6.5 $m^2\ g^{-1}$. They are largely insensitive to the shell thickness because the particle diameters below 0.07 μm are much smaller than the wavelength of light considered here (0.55 μm), and the particles are in the volume-absorption regime [*Bohren and Huffman*, 1983; *Bond et al.*, 2006]. On the other hand, particles larger than 0.07 μm wet diameter show appreciable BC-specific absorption cross sections ranging from 5 to 25 $m^2\ g^{-1}$. Absorption by these particles not only depends on the size but also the BC mass fraction. Consistent with the previously reported calculations [*Fuller et al.*, 1999; *Bond et al.*, 2006, and references therein], the BC-specific absorption of particles of same wet size increased with decreasing BC mass fraction (i.e., increasing coating thickness compared to the BC core diameter). For instance, background particles and cooking POA particles that have coagulated with relatively

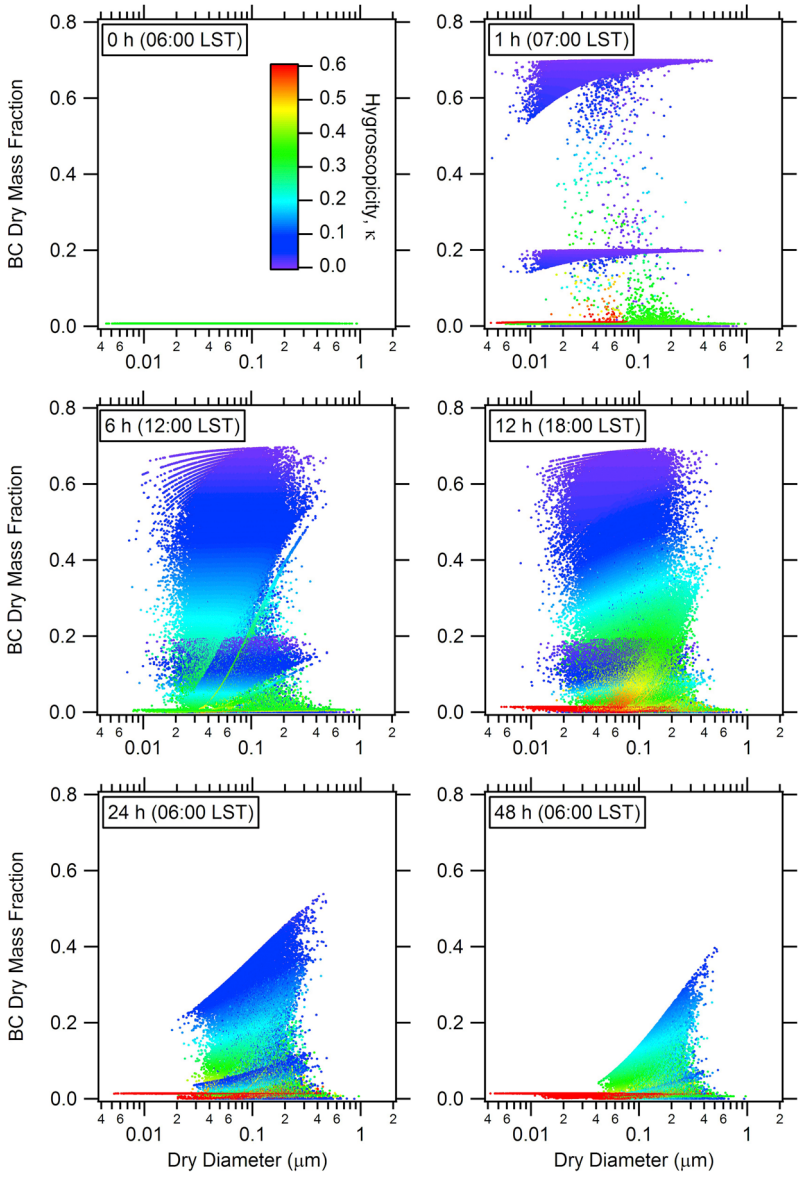

Figure 5. Evolution of BC mass fraction (mixing state) as a function of dry diameter. Each point represents an individual particle and is colored by its hygroscopicity value.

smaller soot particles have the largest BC-specific absorption cross sections (up to 25 $m^2\ g^{-1}$). Gasoline soot particles, which contain 20% or less (when aged) BC by mass, show intermediate-BC-specific absorption cross sections (10–15 $m^2\ g^{-1}$), while diesel soot particles, which contain 70% or less BC, show the lowest values (5–10 $m^2\ g^{-1}$).

[30] The heterogeneity in aerosol mixing states seen in Figure 5 is reflected in Figure 6 by the wide-ranging BC-specific absorption values for particles of same wet diameter. However, sectional aerosol models, which assume all particles within each size bin to be internally mixed, predict a single value of BC-specific absorption for all particles in a given bin. The thick black lines overlaid on the particle-resolved results in Figure 6 depict what the BC-specific absorption would be for 10 logarithmically spaced internally mixed bins (see section 3.2.2). The bins themselves were based on volume mean dry diameter, while the BC-specific absorption for each bin is plotted against wet diameter to be consistent with the particle-resolved results. Also, particles in each bin are assumed to be monodisperse. This bin structure is equivalent to the moving center sectional approach of *Jacobson* [1997].

[31] Figure 7 shows similar results describing the effects of mixing state on the specific scattering cross sections of individual particles. Background aerosol and cooking POA, which contain negligibly small or zero BC, appear as purple dots and show markedly different specific scattering compared to diesel and gasoline soot particles that contain significant amounts of BC. The comparatively large specific scattering of the particles with a small mass fraction of soot, compared to those with much more soot, is a result of the interplay of the scattering efficiency, particle diameter, and particle density. After the soot particles have sufficiently aged and their soot mass fractions decrease, only then do

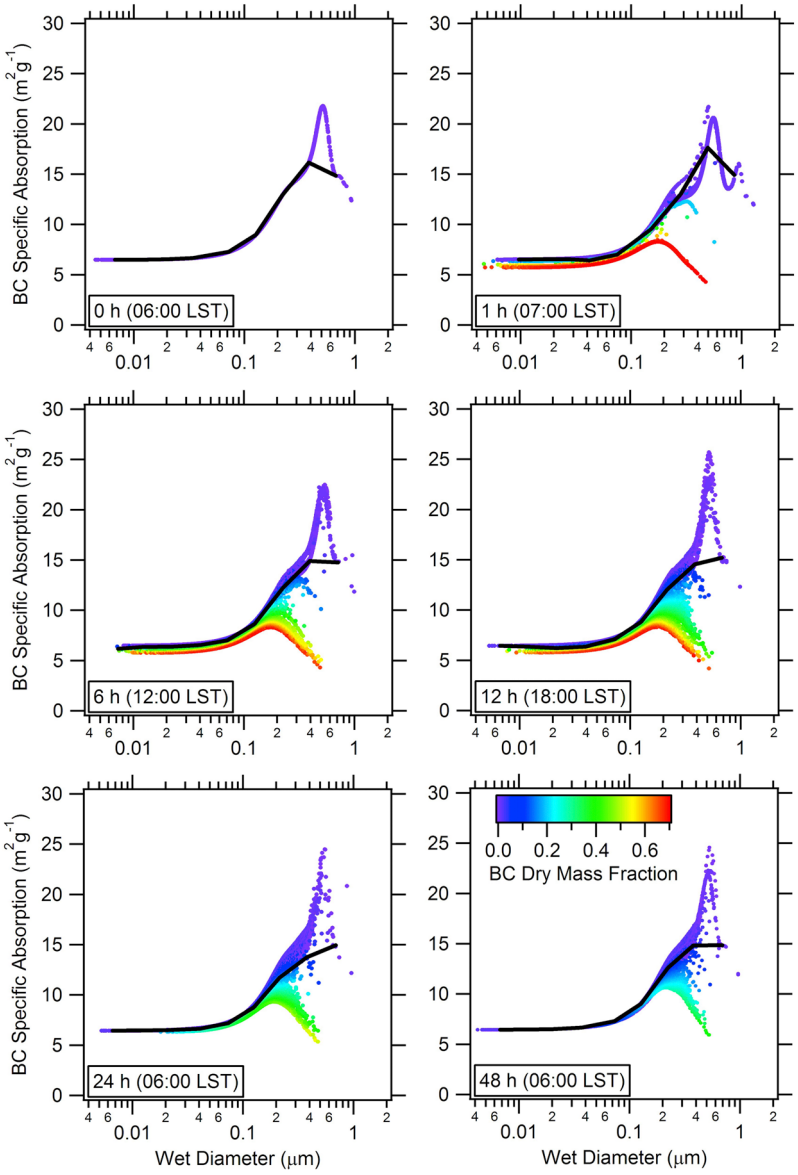

Figure 6. Evolution of BC-specific absorption cross-section area of individual particles as a function of wet diameter. Each point represents an individual particle and is colored by its BC dry mass fraction. The thick black lines represent the BC-specific cross sections if the individual particles were artificially internally mixed over 10 logarithmically spaced size bins.

their specific scattering values begin to increase and move slightly toward the specific scattering values of other non-BC containing particles (e.g., see Figure 7, time equals 48 h). Again, the thick black lines overlaid on the particle-resolved results in Figure 7 depict what the specific scattering cross section would be if the individual particles were artificially internally mixed over 10 logarithmically spaced bins.

3.2.2. Effect of Binning on Ensemble Optical Properties

[32] Figure 8 shows the evolution of ensemble BC-specific absorption and scattering cross sections, ensemble optical coefficients (extinction, scattering, and absorption), ensemble single scattering albedo, and ensemble asymmetry parameter, calculated from the particle-resolved results and the binned results. This comparison provides unprecedented insights into the errors introduced due to the internal mixture assumption as well as due to bin size resolution.

[33] The initial high ensemble BC-specific absorption cross section of 13.4 $m^2\ g^{-1}$ in background aerosol decreases sharply to 7.8 $m^2\ g^{-1}$ as fresh soot particles from diesel and gasoline vehicle exhaust are emitted into the air parcel. The ensemble BC-specific absorption then gradually increases to 10.8 $m^2\ g^{-1}$ over the course of 2 days as the soot particles age due to condensation and coagulation processes. However, since the internal mixture assumption artificially further increases the thickness of nonabsorbing shell in a given bin, the resulting ensemble BC-specific absorption based on internally mixed bins tends to be 30% higher in fresh emissions and 14% higher in the aged air mass than

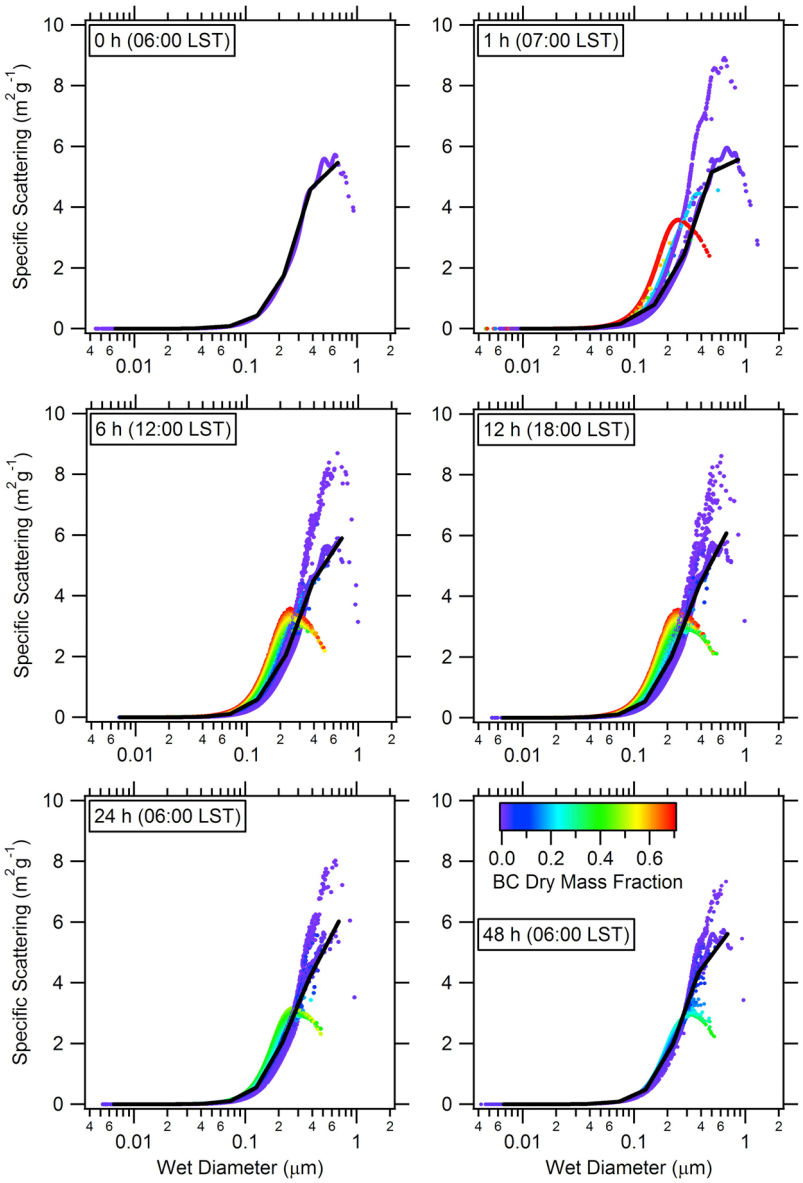

Figure 7. Evolution of specific scattering cross-section area of individual particles as a function of wet diameter. Each point represents an individual particle and is colored by its BC dry mass fraction. The thick black lines represent the specific scattering cross sections if the individual particles were artificially internally mixed over 10 logarithmically spaced size bins.

the ensemble BC-specific absorption based on particle-resolved results. Interestingly, bin resolution (100 versus 10) did not have any noticeable effect on this error. The ensemble specific scattering cross section varied between 2.4 and 3.4 $m^2\ g^{-1}$ over the course of 2 days, but no differences are seen between the particle-resolved and internally mixed bin ensemble results. Moreover, bin resolution (100 versus 10) did not have any noticeable effect on the results either.

[34] Time evolution of ensemble absorption coefficient (B_{abs}) resembles that of bulk BC mass concentration seen previously in Figure 3 and includes the effect of enhanced absorption due to aging. In contrast, time evolution of ensemble scattering (B_{scat}) and extinction (B_{ext}) coefficients follow the combined effects of evolving aerosol nitrate, sulfate, ammonium, SOA, BC, and water concentrations. As with ensemble specific absorption, the internal mixing assumption artificially increased the ensemble absorption coefficients by up to 30% and at least 14% compared to particle-resolved ensemble B_{abs}. However, bin resolution (100 versus 10) did not have any noticeable effect on this bias. On the other hand, negligible differences are seen between particle-resolved and 100 internally mixed bin ensemble B_{scat} values, while the 10 internally mixed bin B_{scat} values are consistently about 10% lower than particle-resolved ensemble B_{scat}. Interestingly, the biases in the internally mixed B_{abs} and B_{scat} nearly cancel each other out, and the resulting internally mixed B_{ext} agrees quite well with particle-resolved ensemble B_{ext}.

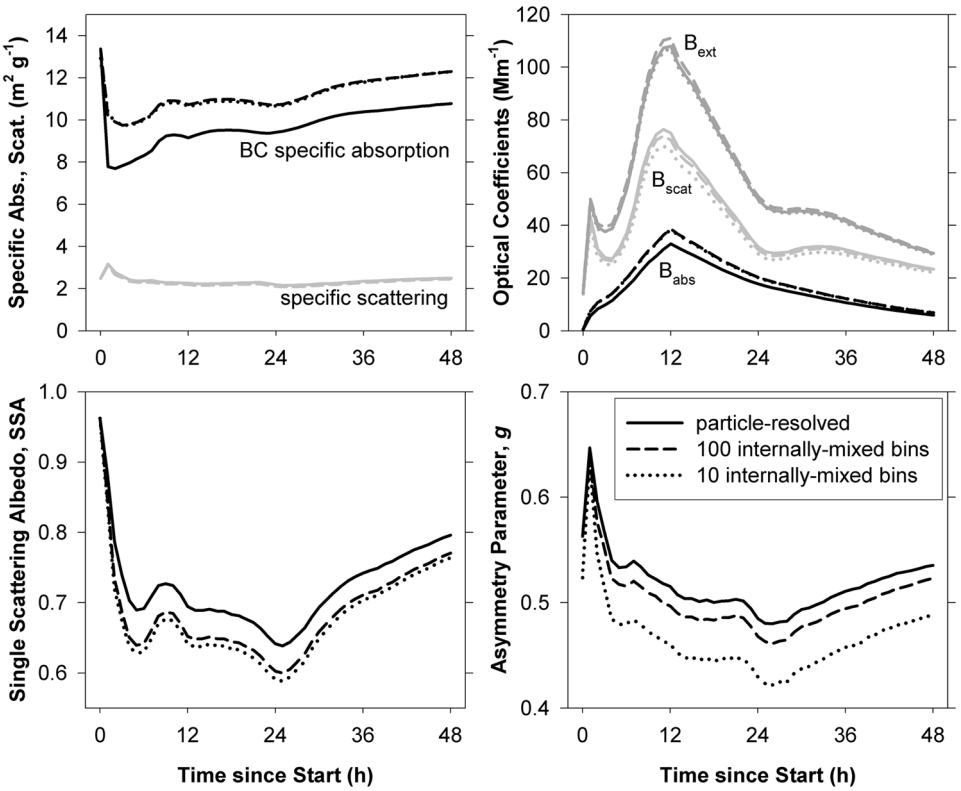

Figure 8. Effect of binning on the evolution of predicted ensemble aerosol optical properties.

[35] The initial high ensemble single scattering albedo of 0.97 decreased rapidly down to 0.7 as diesel and gasoline soot particles are emitted into the air parcel. However, its evolution thereafter depends on a convoluted balance between increase and decease in nonabsorbing species due to condensation and evaporation and increase and decrease in BC mass (due to emission and dilution) and its specific absorption (due to coating by nonabsorbing species). As a result, SSA experienced several local maxima and minima before reaching a value of 0.8 at the end of 2 days. Internal mixture assumption introduced an appreciable negative bias in the ensemble SSA, and the bias is only slightly worse for 10 bins compared to 100 bins. For instance, the 10 bin ensemble SSA is up to 0.07 lower than the particle-resolved ensemble SSA during the first 6 h of the simulation, at least 0.05 during the first 24 h and between 0.04 and 0.03 for the rest of the simulation. The bias in the 100-bin ensemble SSA is only about 0.015 lower than in the 10-bin ensemble SSA.

[36] Our comparison between the particle-resolved and internally mixed sectional approach for SSA exhibits differences that are consistent with those reported by *Oshima et al.* [2009]. As previously mentioned, Oshima *et al.* resolved the BC mixing state and particle size using a two-dimensional bin structure, thereby reducing artificial aging inherent in traditional internally mixed sectional models that resolve only particle size. Their Figure 5 shows a difference in SSA (also for $\lambda = 0.55$ μm) between mixing state resolved approach and the conventional, internally mixed sectional approach. This difference is about 0.06 for their aged particles, a number that is quite similar to ours.

[37] The internal mixture assumption in the present study also introduced noticeable bias in the ensemble asymmetry parameter. For instance, the bias in ensemble g calculated with 10 and 100 internally mixed bins grow with time and are up to −0.06 and −0.02, respectively, by the end of the first 24 h and decrease down to −0.05 and −0.01, respectively, at the end of the 48 h simulation.

[38] *McComiskey et al.* [2008] noted that one of the largest contributors to uncertainties in direct radiative forcing is SSA (i.e., Figure 5 in McComiskey *et al.*; note that they define the overall uncertainty in forcing by a property of interest as the sensitivity of the forcing to changes in the value of the property multiplied by the property's measurement uncertainty). Using the analysis of McComiskey *et al.*, *Chin et al.* [2009] showed that uncertainties in SSA of about 0.02 correspond to uncertainties in instantaneous direct radiative forcing of 1 W m^{-2}. The need to compute SSA to about this level of accuracy suggests that, first, the effect of artificial aging, which introduces errors in SSA calculations of about 0.04 or greater, may be unacceptably large and, second, global models that are used to calculate direct radiative forcing should reliably account for BC mixing state evolution.

3.2.3. Effect of Coagulation on Ensemble Optical Properties

[39] The particle-resolved ensemble optical properties shown in Figure 8 included the effects of both condensation and coagulation. Figure 9 shows the effect of coagulation on the ensemble optical properties by comparing the results from "with coagulation" and "without coagulation" simulations. Both ensemble BC-specific absorption (SA) and

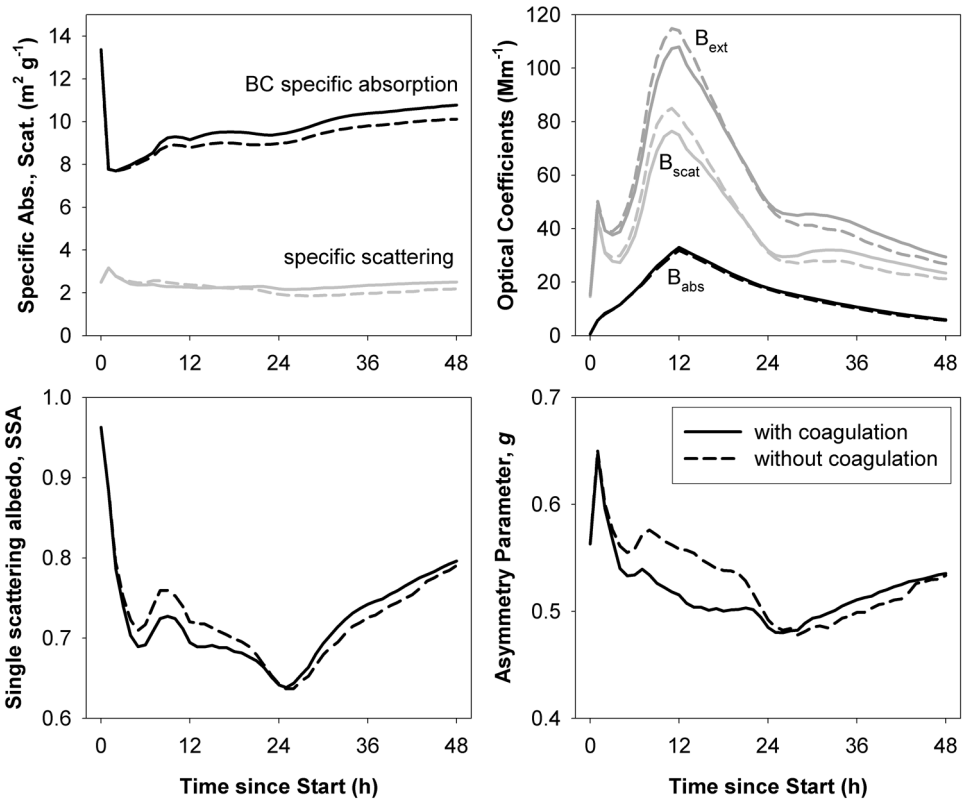

Figure 9. Effect of coagulation on the evolution of predicted ensemble aerosol optical properties.

ensemble specific scattering (SS) cross sections were slightly higher in the simulation with coagulation compared to without coagulation. Coagulation of small particles containing BC with larger ones not only increased the size of the resulting particles but also the internal mixing and hence the ensemble SA as well. Since the concentration of BC mass was nearly identical in simulations with and without coagulation (as was seen in Figure 3), the resulting ensemble B_{abs} was also slightly higher with coagulation than without. Again, the ensemble SS was slightly higher in the simulation with coagulation than without after 24 h because of the larger accumulation mode particles with larger scattering efficiency due to coagulation. However, because the total aerosol mass (especially liquid water) was lower with coagulation than without, the ensemble B_{scat} and B_{ext} were also lower with coagulation than without.

[40] Since the ensemble SA was slightly higher with coagulation than without, while ensemble SS was about the same in both cases during the first 24 h, the differences between the corresponding ensemble SSA values were relatively small but not insignificant. For instance, ignoring coagulation introduced a positive bias in the ensemble SSA of 0.01–0.035 during the first 24 h of plume evolution and a negative bias of less than 0.02 for the subsequent 24 h. Similarly, ignoring coagulation introduced a positive bias of up to 0.05 in the ensemble asymmetry parameter during the first 24 h and a negative bias of ~0.01 during the subsequent 24 h. These biases are largely due to the difference in the water contents predicted with and without coagulation (as was seen in Figure 3).

3.3. Evolution of CCN Activation Properties

3.3.1. Particle-Resolved Results

[41] Figure 10 shows the time evolution of the particle-resolved critical supersaturation spectrum as a function of dry diameter. Again, the points are colored by their BC dry mass fractions. Thin black lines mark the constant hygroscopicity values: κ = 0, 0.001, 0.01, 0.1, and 1. The thick black line overlaid on the particle-resolved results in each plot depict what the critical supersaturations would be if the individual particles were artificially internally mixed over 10 logarithmically spaced dry diameter bins. Again, particles in each bin are assumed to be monodisperse at volume mean dry diameter. At the start of the simulation, all particles have the same composition and hence the same hygroscopicity value, so the particle-resolved results are indistinguishable from the 10 internally mixed bin results. With the emission of diesel and gasoline soot and cooking POA, particles with significantly different BC dry mass fractions emerge in these plots. However, because all of these particles are hydrophobic to begin with (κ = 0.001), they frequently appear on top of each other in these plots despite their differences in BC dry mass fractions. In other words, BC dry mass fraction is not a unique indicator of particle hygroscopicity.

[42] As these different hydrophobic particles age due to condensation and coagulation, their dry size and overall hygroscopicity values increase and, as a result, their critical supersaturation values decrease. However, significant heterogeneity in aerosol mixing states and overall particle

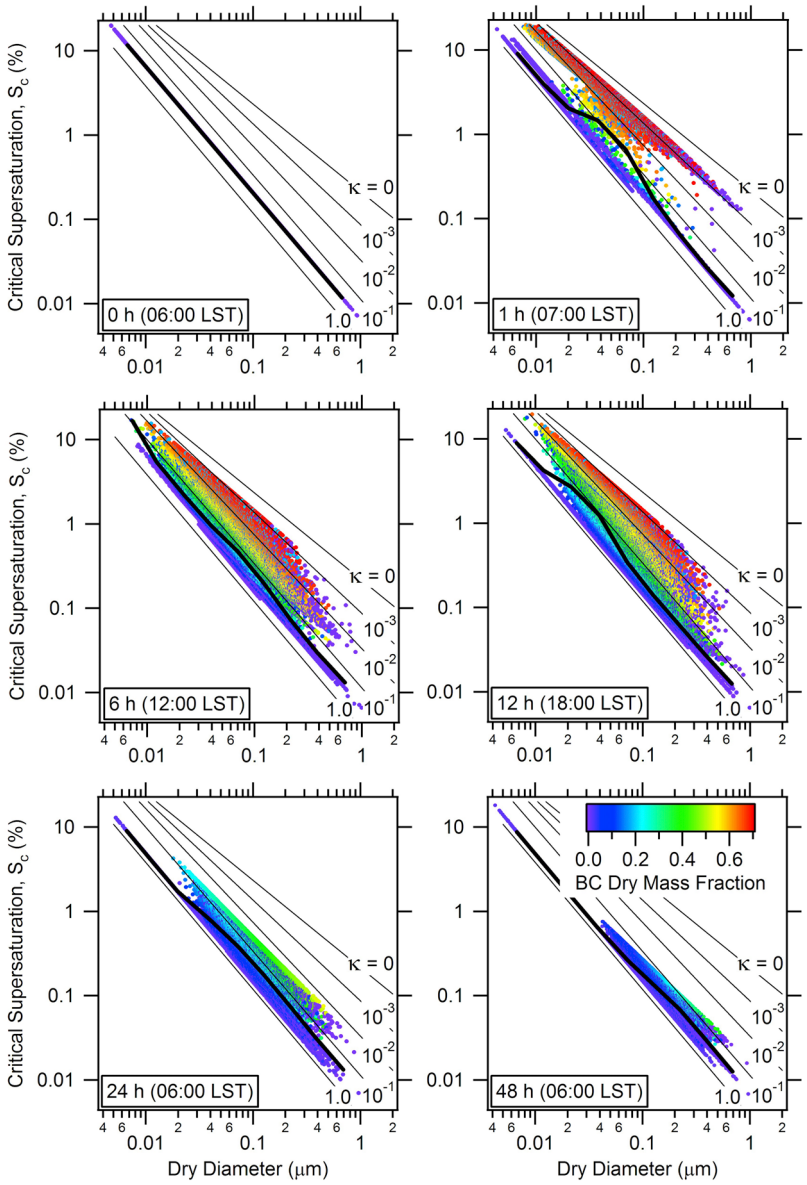

Figure 10. Evolution of critical supersaturation for individual particles as a function of their dry diameter. Each point represents an individual particle and is colored by its BC dry mass fraction. The thick black lines represent the critical supersaturations if the individual particles were artificially internally mixed over 10 logarithmically spaced size bins.

hygroscopicity values persists in the air parcel until the fresh emissions stop at 1800 LST on the first day. After 2 days of aging, the range in hygroscopicity values of aerosols is significantly reduced (between ~0.1 and 0.6) even though appreciable differences in the composition (not just BC mass fraction) of individual particles still exist. For this aged aerosol, the exact chemical composition appears to matter less than the size of the particles as far as their CCN activation properties are concerned. While this view is consistent with *Dusek et al.* [2006], it is evident that the aging of the freshly emitted primary aerosols, which makes them hygroscopic and efficient CCN, could not have occurred without condensational growth. Consistent with *Jacobson* [2002], we find that many of the particles are affected by coagulation. At 24 h, 48% of the particles have experienced coagulation, and these coagulated particles consist of 3.1 original particles (on average). As also noted in the work of *Jacobson* [2002], many of the coagulation events involve a smaller and a larger particle. These events produce small changes to the properties of the resulting larger particles and have limited impact on mixing state heterogeneity.

[43] From the position of the thick black lines relative to the particle-resolved results, it appears that artificial aging of particles due to internally mixed binning generally tends to bias the bin hygroscopicity values toward the high end on the logarithmic κ scale, especially during the first 12 h of the simulation. The effects of binning and bin resolution on the errors in the predicted CCN/CN ratio are discussed next.

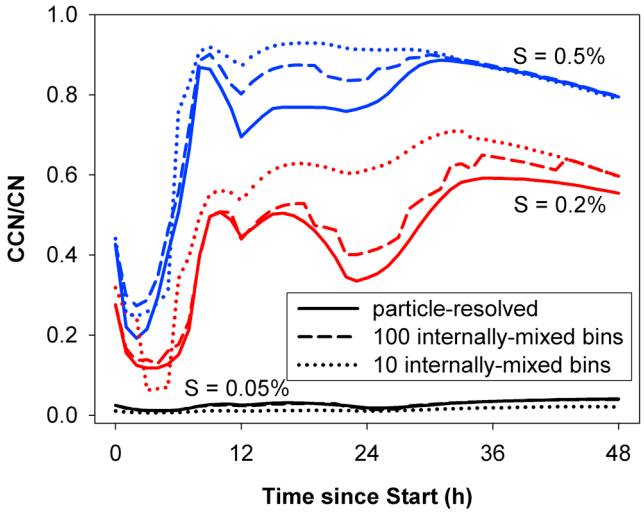

Figure 11. Effect of binning on the predicted evolution of CCN/CN ratios at three different supersaturations.

3.3.2. Effect of Binning on CCN/CN Ratio

[44] Figure 11 shows time evolution of CCN/CN ratio for three different supersaturations (S = 0.05%, 0.2%, and 0.5%), calculated directly from the particle-resolved results and after binning to 100 or 10 internally mixed bins. The initial CCN/CN ratio for a given S_c decreases sharply as fresh diesel and gasoline soot and POA particles are emitted into the air parcel. Rapid aging of these primary particles by condensation and coagulation causes the CCN/CN ratio for each S to go though a minimum within ~3 h and peak after about 9 h from start. However, with the slowdown of photochemical production of condensable gases by late afternoon coupled with continued evaporation of NH_4NO_3 due to dilution, the CCN/CN ratios decrease again and go through local minima before they increase again the following morning.

[45] Since internally mixed binning artificially renders freshly emitted soot and POA particles hygroscopic, it tends to overpredict the CCN/CN ratio compared to the particle-resolved results, except in cases with very low supersaturations. For S = 0.5%, the CCN/CN ratio using 100 internally mixed bins is about 40% higher than the particle-resolved results during the first 3 h of simulation (0600–0900 LST), when particle growth by condensation is slow. From 4 to 11 h simulation time (1000–1700 LST), when condensation is more rapid, the bias decreases to less than 10% and the bias increases to about 10–15% over the night when aging by condensation nearly stops. After 30 h, the 100-bin results are very close to the particle resolved results. With 10 internally mixed bin results, the biases are about 20% out to 30 h. After 30 h, the 10-bin results are also very close to the particle-resolved results.

[46] For S = 0.2%, the 100-bin results show similar biases relative to the particle-resolved results. In the first 6 h, the maximum bias is only 25%, as the artificial internal mixing classifies fewer of the freshly emitted particles as CCN at this S. The bias generally stays at less than 10% (maximum 20%) through most of the remainder of the simulation. With 10 bins, the biases are substantially higher, reaching as high as 125% during the first 6 h, decreasing to 20% at 12 h, and then increasing to 80% at the end of first 24 h period. The bias gradually decreased thereafter and was less than 10% at the end of the simulation (48 h).

[47] For S = 0.05%, the CCN/CN ratios predicted using 100 internally mixed bins are about 4% lower on average (maximum 25%) than the particle-resolved results. This underprediction occurs because when highly hygroscopic, submicron-sized background particles, which readily activate 0.05% supersaturation, are artificially internally mixed with freshly emitted particles with very low hygroscopicity, the resulting particles with mean hygroscopicity may no longer activate at the same supersaturation. With 10 bins, the CCN/CN ratios are 40–60% lower than the particle-resolved results, and this much greater bias can again be attributed to coarse size resolution effects.

[48] The results for S = 0.2% and 0.5% are qualitatively consistent with the model analysis of field observations by *Cubison et al.* [2008], who showed that it is necessary to resolve the aerosol mixing state in order to correctly predict the CCN concentrations in a polluted urban environment where aged particles (containing inorganic and SOA species) are externally mixed with freshly emitted soot and POA. They found a much stronger effect, with CCN predicted with the internal mixing assumption being a factor of 3 greater than observed at 0.5% S. In our simulation, the internal mixing assumption (with 100 bins) overpredicts CCN (compared to the particle-resolved results) by about 40% during the first few hours of simulation, but this bias drops to about 10% the remainder of the first day. The lower bias here compared to the work of *Cubison et al.* [2008] can be attributed to the rapid aging of fresh particles by condensation, and this aging is apparently more rapid in our simulation than under the conditions of the Cubison *et al.* study.

[49] The much larger biases with 10 internally mixed bins are primarily due to the coarse size resolution and the use of the moving center representation for calculating CCN concentrations. Because all particles in each bin are assumed to be monodisperse at the volume mean $D_{p,dry}$, either all or none of the particles in a bin activate at a given supersaturation. With coarse size resolution, the resulting cumulative CCN distribution has a distinctly stair-step appearance. Using a different numerical method that produces a smoother CCN distribution (e.g., the linear discrete approach of *Simmel and Wurzler* [2006]) could reduce the biases associated with size resolution.

3.3.3. Effect of Coagulation on CCN Concentration

[50] Figure 12 shows the effect of coagulation on CCN number concentration evolution at S = 0.05%, 0.2%, and 0.5%. According to the particle-resolved results seen previously in Figure 10, only particles larger than ~0.2 and ~0.08 μm would activate with supersaturations of 0.05% and 0.2%, respectively. Also, according to the number size distributions seen previously in Figure 4, the number concentrations of particles larger than ~0.2 μm were essentially indistinguishable between the simulations with and without coagulation. Consequently, negligible bias is seen in the CCN concentrations at S = 0.05% when coagulation was ignored. On the other hand, significant reductions in the number concentrations were seen for particles 0.2 μm and

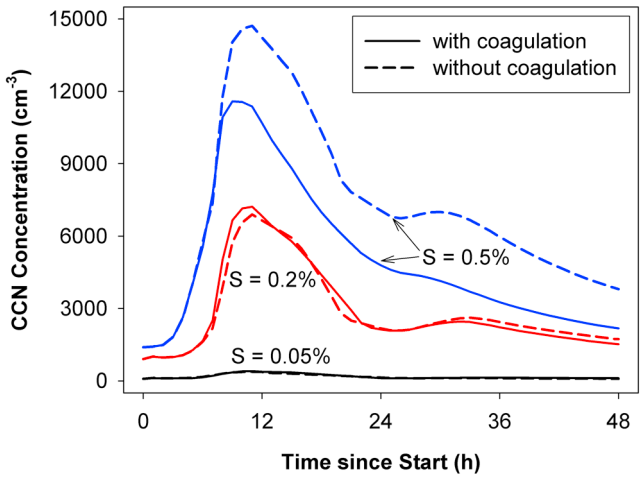

Figure 12. Effect of coagulation on the predicted evolution of CCN concentrations at three different supersaturations.

smaller due to coagulation. An appreciable fraction of CCN at S = 0.2% are particles smaller than 0.2 μm. The CCN concentration at 0.2% is therefore expected to decrease when coagulation is included due to the associated reductions in the number concentrations of particles smaller than 0.2 μm. However, coagulation tends to increase internal mixing and the resulting average hygroscopicity of particles and hence the CCN concentration. These opposing effects appear to nearly compensate each other in the present scenario as seen in the CCN plot for S = 0.2% in Figure 4. Finally, since particles smaller than 0.2 μm require higher supersaturations to activate, large positive biases in the CCN concentrations at S = 0.5% were introduced by ignoring coagulation. The bias was about 25% after first 10 h and steadily grew to about 80% at the end of 2 days of evolution.

4. Summary, Implications, and Future Work

[51] The recently developed particle-resolved aerosol box model PartMC-MOSAIC was used to simulate the evolution of aerosol mixing state and the associated optical and cloud condensation nuclei (CCN) activation properties in an idealized large urban plume for a period of 2 days. The model explicitly resolved the size and composition of individual particles in an external mixture of diesel soot, gasoline soot, cooking organic aerosol, and background aerosol and tracked their evolution due to condensation, evaporation, coagulation, emission, and dilution. Over the course of the simulation the mixing state of freshly emitted particles changed significantly as a result of coagulation and condensation over the entire size range, consistent with the work of *Jacobson* [2002]. Significant heterogeneity in aerosol mixing state was predicted even after 1–2 days of aging, which was reflected in the wide range of BC-specific absorption cross sections and critical supersaturations predicted for particles of same wet and dry diameters, respectively.

[52] The ensemble black carbon (BC) specific absorption cross section increased by 40% over the course of 2 days as a result of BC aging by condensation and coagulation. In contrast, threefold and fourfold enhancements in CCN/CN ratios were predicted to occur within 6 h for 0.2% and 0.5% supersaturations, respectively. The particle-resolved results were then used to evaluate the errors in the predicted optical and CCN activation properties in a conventional sectional framework, which typically assumes monodisperse, internally mixed particles within each bin. The analysis showed that this assumption artificially increased the ensemble BC-specific absorption by 14–30% and decreased the single scattering albedo (SSA) by 0.03–0.07, while the bin size resolution had a negligible effect.

[53] Coagulation reduced the number concentrations of particles smaller than 0.2 μm diameter by 50% over the course of 2 days. Also, particles formed as a result of coagulation of metastable (liquid) particles with stable dry particle (solid) were assumed to take the thermodynamically stable phase state as dictated by the new composition, ambient RH, and temperature. Neglecting coagulation therefore overpredicted liquid water as well as the number concentration of particles smaller than 0.2 μm diameter. The error in the water content and hence in particle size and refractive index introduced a positive bias in the ensemble SSA of 0.01–0.035 during the first 24 h of plume evolution and a negative bias of less than 0.02 for the subsequent 24 h. A positive bias of up to 0.05 was introduced in the ensemble asymmetry parameter during the first 24 h and a negative bias of ~0.01 during the second 24 h. Neglecting coagulation produced negligible bias in the CCN concentrations at S = 0.05 and 0.2% supersaturations, while large positive biases (25–80%) were seen at S = 0.5%.

[54] According to these results, significant heterogeneity in aerosol mixing state may be expected in large urban plumes even after 1–2 days of aging. Potentially significant errors or biases in the modeled aerosol direct radiative forcing (DRF) on a regional scale could therefore be introduced if the aerosol mixing state evolution due to condensation and coagulation is not adequately resolved in the model. For instance, *McComiskey et al.* [2008] noted that in most situations one of the largest contributors to uncertainties in direct radiative forcing (DRF) is the SSA. Using the analysis of McComiskey *et al.*, *Chin et al.* [2009] showed that uncertainties in instantaneous DRF of 1 W m^{-2} correspond to uncertainties in SSA of about 0.02. The need to compute SSA to about this level of accuracy suggests that the effect of artificial aging due to the internal mixture assumption, which introduces biases in SSA of about 0.05 or greater, may be unacceptably large. Regional and global climate models that are used to calculate DRF should therefore account for the evolution of BC mixing state.

[55] Many studies have shown that mixing state heterogeneity also affects CCN and thus aerosol indirect radiative forcing. *Pierce et al.* [2007] explored the global sensitivity of CCN to aerosol mixing state and found that globally the sensitivity to mixing state was negligible as long as the organics are generally soluble. *Sotiropoulou et al.* [2007] found that CCN uncertainties of 10–20% (resulting from mixing state uncertainty) produced indirect radiative forcing uncertainties of 10–20% both globally and regionally and concluded that this was not a significant source of error for modeling the aerosol indirect effect. Clearly, a larger uncertainty in CCN would produce a larger uncertainty in indirect forcing. In our simulations, ignoring mixing state

heterogeneity (by assuming 100 internally mixed bins) caused CCN at 0.5% S to be overestimated by 40% during the first few hours of simulation and 10% out to about 30 h. These overestimates are considerably lower than those from the work of *Cubison et al.* [2008] for an urban location and are somewhat lower than those from the work of *Medina et al.* [2007] for a site in SE New Hampshire, which suggests that our results are conservative. We found larger biases with 10 internally mixed bins, but these were partially due to size resolution issues rather than mixing state. These results suggest that additional scenarios and sensitivity studies are needed to better understand what conditions (aerosol and precursor gas emissions) produce the large effects such as found by *Cubison et al.* [2008]. Additional scenarios and sensitivity studies are also needed to investigate the ability of complex mixing state representations within sectional (and modal) framework to reliably predict optical and CCN properties. As part of future studies, it is also necessary to evaluate the effects of homogeneous nucleation, aging POA, and aqueous phase chemistry under different scenarios in the evolution of aerosol mixing state and optical and CCN properties.

[56] Quantitative measurements of particle-resolved size and composition are required to effectively constrain, evaluate, and improve the representation of different types of aerosols and their optical and CCN activation properties in the PartMC-MOSAIC model. Several state-of-the-art instruments such as PALMS [*Murphy and Thomson*, 1997], ATOFMS [*Moffet and Prather*, 2005; *Spencer and Prather*, 2006], SPLAT [*Zelenyuk and Imre*, 2005; *Zelenyuk et al.*, 2009], LS-ToF-AMS [*Cross et al.*, 2009], and SP2 [*Baumgardner et al.*, 2004; *Schwarz et al.*, 2006; *Moteki et al.*, 2007] can provide single-particle composition and mixing state information. It is also possible to obtain density, morphology, and hygroscopicity [*Zelenyuk et al.*, 2008a, 2008b, 2008c], scattering cross sections [*Moffet et al.*, 2008], and absorption cross sections [*Subramanian et al.*, 2010] of aerosols as function of particle size and mixing state. Data from these instruments along with traditional CCN and optical properties measurements can potentially be used to meet the critical model development and evaluation needs, and plans for focused laboratory and field studies with these objectives are underway. The ultimate goal of such an integrated particle-resolved modeling and measurement strategy is to develop and evaluate a reliable and computationally efficient mixing state framework that can be used in regional and global climate models.

[57] **Acknowledgments.** Funding for R. A. Zaveri, J. C. Barnard, and R. C. Easter was provided by the Aerosol-Climate Initiative as part of the Pacific Northwest National Laboratory (PNNL) Laboratory Directed Research and Development (LDRD) program. Funding for N. Riemer and M. West was provided by the National Science Foundation (NSF) under grant ATM 0739404 and CMG 0934491. N. Riemer also acknowledges funding from the NASA MAP program, grant NNX09AK66G. Pacific Northwest National Laboratory is operated for the U.S. Department of Energy by Battelle Memorial Institute under contract DE-AC06-76RLO 1830.

References

Ackerman, T. P., and O. B. Toon (1981), Absorption of visible radiation in atmospheres containing mixtures of absorbing and nonabsorbing particles, *Appl. Opt.*, *20*, 3661–3668, doi:10.1364/AO.20.003661.

Bauer, S. E., D. L. Wright, D. Koch, E. R. Lewis, R. McGraw, L. S. Chang, S. E. Schwartz, and R. Rued (2008), MATRIX (Multiconfiguration Aerosol TRacker of mIXing state): An aerosol microphysical module for global atmospheric models, *Atmos. Chem. Phys.*, *8*, 6003–6035, doi:10.5194/acp-8-6003-2008.

Baumgardner, D., G. Kok, and G. Raga (2004), Warming of the Arctic lower stratosphere by light absorbing particles, *Geophys. Res. Lett.*, *31*, L06117, doi:10.1029/2003GL018883.

Bohren, C. F., and D. R. Huffman (1983), *Absorption and Scattering of Light by Small Particles*, John Wiley, New York.

Bond, T. C., and R. W. Bergstrom (2006), Light absorption by carbonaceous particles: An investigative review, *Aerosol Sci. Technol.*, *40*, 27–67, doi:10.1080/02786820500421521.

Bond, T. C., G. Habib, and R. W. Bergstrom (2006), Limitations in the enhancement of visible light absorption due to mixing state, *J. Geophys. Res.*, *111*, D20211, doi:10.1029/2006JD007315.

Cantrell, W., G. Shaw, G. R. Cass, Z. Chowdhury, L. S. Hughes, K. A. Prather, S. A. Guazzotti, and K. R. Coffee (2001), Closure between aerosol particles and cloud condensation nuclei at Kaashidhoo Climate Observatory, *J. Geophys. Res.*, *106*, 28,711–28,718, doi:10.1029/2000JD900781.

Capaldo, K. P., C. Pilinis, and S. N. Pandis (2000), A computationally efficient hybrid approach for dynamic gas/aerosol transfer in air quality models, *Atmos. Environ.*, *34*, 3617–3627, doi:10.1016/S1352-2310(00)00092-3.

Chin, M., R. A. Kahn, D. Rind, G. Feingold, S. E. Schwartz, and P. DeCola (Eds.) (2009), *Atmospheric Aerosol Properties and Climate Impacts, A Report by the U.S. Climate Change Science Program and the Subcommittee on Global Change Research*, *SAP 2.3*, NASA, Washington, D. C.

Cross, E. S., T. B. Onasch, M. Canagaratna, J. T. Jayne, J. Kimmel, X.-Y. Yu, M. L. Alexander, D. R. Worsnop, and P. Davidovits (2009), Single particle characterization using a light scattering module coupled to a time-of-flight aerosol mass spectrometer, *Atmos. Chem. Phys.*, *9*, 7769–7793, doi:10.5194/acp-9-7769-2009.

Cubison, M. J., B. Ervens, G. Feingold, K. S. Docherty, I. M. Ulbrich, L. Shields, K. Prather, S. Hering, and J. L. Jimenez (2008), The influence of chemical composition and mixing state of Los Angeles urban aerosol on CCN number and cloud properties, *Atmos. Chem. Phys.*, *8*, 5649–5667, doi:10.5194/acp-8-5649-2008.

Delene, D. J., and J. A. Ogren (2002), Variability of aerosol optical properties at four North American surface monitoring sites, *J. Atmos. Sci.*, *59*, 1135–1150, doi:10.1175/1520-0469(2002)059<1135:VOAOPA>2.0.CO;2.

Dubovik, A., B. Holben, T. F. Eck, A. Smirnov, Y. J. Kaufman, M. D. King, D. Tanré, and I. Slutsker (2002), Variability of absorption and optical properties of key aerosol types observed in worldwide locations, *J. Atmos. Sci.*, *59*, 590–608, doi:10.1175/1520-0469(2002)059<0590:VOAAOP>2.0.CO;2.

Dusek, U., et al. (2006), Size matters more than chemistry for cloud-nucleating ability of aerosol particles, *Science*, *312*, 1375–1378, doi:10.1126/science.1125261.

Fassi-Fihri, A., K. Suhre, and R. Rosset (1997), Internal and external mixing in atmospheric aerosols by coagulation: Impact on the optical and hygroscopic properties of the sulphate-soot system, *Atmos. Environ.*, *31*, 1393–1402, doi:10.1016/S1352-2310(96)00341-X.

Forster, P. V., et al. (2007), Changes in Atmospheric Constituents and in Radiative Forcing, in *Climate Change 2007: The Physical Science Basis: Working Group I Contribution to the Fourth Assessment Report of the IPCC*, edited by S. Solomon, et al., pp. 129–234, Cambridge Univ. Press, New York.

Fuller, K. A., W. C. Malm, and S. M. Kreidenweis (1999), Effects of mixing on extinction by carbonaceous particles, *J. Geophys. Res.*, *104*, 15,941–15,954, doi:10.1029/1998JD100069.

Furutani, H., M. Dall'osto, G. C. Roberts, and K. A. Prather (2008), Assessment of the relative importance of atmospheric aging on CCN activity derived from field observations, *Atmos. Environ.*, *42*, 3130–3142, doi:10.1016/j.atmosenv.2007.09.024.

Ghan, S. J., and S. E. Schwartz (2007), Aerosol properties and processes—A path from field and laboratory measurements to global climate models, *Bull. Am. Meteorol. Soc.*, *88*, 1059–1083, doi:10.1175/BAMS-88-7-1059.

Ghan, S. J., N. S. Laulainen, R. C. Easter, R. Wagener, S. Nemesure, E. G. Chapman, Y. Zhang, and L. R. Leung (2001), Evaluation of aerosol direct radiative forcing in MIRAGE, *J. Geophys. Res.*, *106*, 5317–5334, doi:10.1029/2000JD900501.

Houghton, J. T., Y. Ding, D. J. Griggs, M. Noguer, P. van der Linden, X. Dai, K. Maskell, and C. A. Johnson (Eds.) (2001), *Climate Change 2001: The Scientific Basis*, 881 pp., Cambridge Univ. Press, U. K.

Jacobson, M. Z. (1997), Development and application of a new air pollution modeling system: Part II. Aerosol module structure and design, *Atmos. Environ.*, *31*, 131–144, doi:10.1016/1352-2310(96)00202-6.

Jacobson, M. Z. (2001), Strong radiative heating due to the mixing state of black carbon in atmospheric aerosols, *Nature*, *409*, 695–697, doi:10.1038/35055518.

Jacobson, M. Z. (2002), Analysis of aerosol interactions with numerical techniques for solving coagulation, nucleation, condensation, dissolution, and reversible chemistry among multiple size distributions, *J. Geophys. Res.*, *107*(D19), 4366, doi:10.1029/2001JD002044.

Jacobson, M. Z. (2003), Development of mixed-phase clouds from multiple aerosol size distributions and the effect of the clouds on aerosol removal, *J. Geophys. Res.*, *108*(D8), 4245, doi:10.1029/2002JD002691.

Jacobson, M. Z., R. P. Turco, E. J. Jensen, and O. B. Toon (1994), Modeling coagulation among particles of different composition and size, *Atmos. Environ.*, *28*, 1327–1338, doi:10.1016/1352-2310(94)90280-1.

Kleeman, M. J., et al. (1997), Modeling the airborne particle complex as a source-oriented external mixture, *J. Geophys. Res.*, *102*, 21,355–21,372, doi:10.1029/97JD01261.

Kleinman, L. I., et al. (2007), Aircraft observations of aerosol composition and ageing in New England and Mid-Atlantic States during the summer 2002 New England Air Quality Study field campaign, *J. Geophys. Res.*, *112*, D09310, doi:10.1029/2006JD007786.

Kuwata, M., Y. Kondo, M. Mochida, N. Takegawa, and K. Kawamura (2007), Dependence of CCN activity of less volatile particles on the amount of coating observed in Tokyo, *J. Geophys. Res.*, *112*, D11207, doi:10.1029/2006JD007758.

Lacis, A. A., and M. J. Mishchenko (1995), Climate forcing, sensitivity, and response, in *Aerosol Forcing of Climate*, edited by R. J. Charlson and J. Heintzenberg, pp. 11–42, John Wiley, New York.

Lesins, G., P. Chylek, and U. Lohmann (2002), A study of internal and external mixing scenarios and its effect on aerosol optical properties and direct radiative forcing, *J. Geophys. Res.*, *107*(D10), 4094, doi:10.1029/2001JD000973.

McComiskey, A., S. E. Schwartz, B. Schmid, H. Guan, E. R. Lewis, P. Ricchiazzi, and J. A. Ogren (2008), Direct aerosol forcing: Calculation from observables and sensitivity to inputs, *J. Geophys. Res.*, *113*, D09202, doi:10.1029/2007JD009170.

Medina, J., A. Nenes, R.-E. P. Sotiropoulou, L. D. Cottrell, L. D. Ziemba, P. J. Beckman, and R. J. Griffin (2007), Cloud condensation nuclei closure during the International Consortium for Atmospheric Research on Transport and Transformation 2004 campaign: Effects of size-resolved composition, *J. Geophys. Res.*, *112*, D10S31, doi:10.1029/2006JD007588.

Mochida, M., M. Kuwata, T. Miyakawa, N. Takegawa, K. Kawamura, and Y. Kondo (2006), Relationship between hygroscopicity and cloud condensation nuclei activity for urban aerosols in Tokyo, *J. Geophys. Res.*, *111*, D23204, doi:10.1029/2005JD006980.

Moffet, R. C., and K. A. Prather (2005), Extending ATOFMS measurements to include refractive index and density, *Anal. Chem.*, *77*, 6535–6541, doi:10.1021/ac0503097.

Moffet, R. C., X. Qin, T. Rebotier, H. Furutani, and K. A. Prather (2008), Chemically segregated optical and microphysical properties of ambient aerosols measured in a single-particle mass spectrometer, *J. Geophys. Res.*, *113*, D12213, doi:10.1029/2007JD009393.

Moteki, N., Y. Kondo, Y. Miyazaki, N. Takegawa, Y. Komazaki, G. Kurata, T. Shirai, D. R. Blake, T. Miyakawa, and M. Koike (2007), Evolution of mixing state of black carbon particles: Aircraft measurements over the western Pacific in March 2004, *Geophys. Res. Lett.*, *34*, L11803, doi:10.1029/2006GL028943.

Murphy, D. M., and D. S. Thomson (1997), Chemical composition of single aerosol particles at Idaho Hill: Negative ion measurements, *J. Geophys. Res.*, *102*, 6353–6368, doi:10.1029/96JD00859.

Oshima, N., M. Koike, Y. Zhang, and Y. Kondo (2009), Aging of black carbon in outflow from anthropogenic sources using a mixing state resolved model: 2. Aerosol optical properties and cloud condensation nuclei activities, *J. Geophys. Res.*, *114*, D18202, doi:10.1029/2008JD011681.

Petters, M. D., and S. M. Kreidenweis (2007), A single parameter representation of hygroscopic growth and cloud condensation nucleus activity, *Atmos. Chem. Phys.*, *7*, 1961–1971, doi:10.5194/acp-7-1961-2007.

Pierce, J. R., K. Chen, and P. J. Adams (2007), Contribution of primary carbonaceous aerosol to cloud condensation nuclei: Processes and uncertainties evaluated with a global aerosol microphysics model, *Atmos. Chem. Phys.*, *7*, 5447–5466, doi:10.5194/acp-7-5447-2007.

Riemer, N., M. West, R. A. Zaveri, and R. C. Easter (2009), Simulating the evolution of soot mixing state with a particle-resolved aerosol model, *J. Geophys. Res.*, *114*, D09202, doi:10.1029/2008JD011073.

Riemer, N., M. West, R. A. Zaveri, and R. C. Easter (2010), Estimating black carbon aging time-scales with a particle-resolved aerosol model, *J. Aerosol Sci.*, *41*, 143–158, doi:10.1016/j.jaerosci.2009.08.009.

Russell, L. M., and J. H. Seinfeld (1998), Size- and composition-resolved externally mixed aerosol model, *Aerosol Sci. Technol.*, *28*, 403–416, doi:10.1080/02786829808965534.

Saathoff, H., et al. (2003), Coating of soot and $(NH_4)_2SO_4$ particles by ozonolysis products of α-pinene, *J. Aerosol Sci.*, *34*, 1297–1321, doi:10.1016/S0021-8502(03)00364-1.

Schell, B., I. J. Ackermann, H. Hass, F. S. Binkowski, and A. Ebel (2001), Modeling the formation of secondary organic aerosol within a comprehensive air quality model system, *J. Geophys. Res.*, *106*, 28,275–28,293, doi:10.1029/2001JD000384.

Schnaiter, M., H. Horvath, O. Möhler, K.-H. Naumann, H. Saathoff, and O. Schöck (2003), UV-VIS-NIR spectral optical properties of soot and soot-containing aerosols, *J. Aerosol Sci.*, *34*, 1421–1444, doi:10.1016/S0021-8502(03)00361-6.

Schwarz, J. P., et al. (2006), Single-particle measurements of midlatitude black carbon and light-scattering aerosols from the boundary layer to the lower stratosphere, *J. Geophys. Res.*, *111*, D16207, doi:10.1029/2006JD007076.

Simmel, M., and S. Wurzler (2006), Condensation and activation in sectional cloud microphysical models, *Atmos. Res.*, *80*, 218–236, doi:10.1016/j.atmosres.2005.08.002.

Sotiropoulou, R.-E. P., A. Nenes, P. J. Adams, and J. H. Seinfeld (2007), Cloud condensation nuclei prediction error from application of Köhler theory: Importance for the aerosol indirect effect, *J. Geophys. Res.*, *112*, D12202, doi:10.1029/2006JD007834.

Spencer, M. T., and K. A. Prather (2006), Using ATOFMS to determine OC/EC mass fractions in particles, *Aerosol Sci. Technol.*, *40*, 585–594, doi:10.1080/02786820600729138.

Stier, P., et al. (2005), The aerosol-climate model ECHAM5-HAM, *Atmos. Chem. Phys.*, *5*, 1125–1156, doi:10.5194/acp-5-1125-2005.

Subramanian, R., et al. (2010), Black carbon over Mexico: The effect of atmospheric transport on mixing state, mass absorption cross-section, and BC/CO ratios, *Atmos. Chem. Phys.*, *10*, 219–237, doi:10.5194/acp-10-219-2010.

Volkamer, R., J. L. Jimenez, F. San Martini, K. Dzepina, Q. Zhang, D. Salcedo, L. T. Molina, D. R. Worsnop, and M. J. Molina (2006), Secondary organic aerosol formation from anthropogenic air pollution: Rapid and higher than expected, *Geophys. Res. Lett.*, *33*, L17811, doi:10.1029/2006GL026899.

Wexler, A. S., F. W. Lurmann, and J. H. Seinfeld (1994), Modelling urban and regional aerosols. Part I: Model development, *Atmos. Environ.*, *28*, 531–546, doi:10.1016/1352-2310(94)90129-5.

Wilson, J., C. Cuvelier, and F. Raes (2001), A modeling study of global mixed aerosol fields, *J. Geophys. Res.*, *106*, 34,081–34,108, doi:10.1029/2000JD000198.

Zaveri, R. A., and L. K. Peters (1999), A new lumped structure photochemical mechanism for large-scale applications, *J. Geophys. Res.*, *104*, 30,387–30,415, doi:10.1029/1999JD900876.

Zaveri, R. A., R. C. Easter, and A. S. Wexler (2005a), A new method for multicomponent activity coefficients of electrolytes in aqueous atmospheric aerosols, *J. Geophys. Res.*, *110*, D02201, doi:10.1029/2004JD004681.

Zaveri, R. A., R. C. Easter, and L. K. Peters (2005b), A computationally efficient multicomponent equilibrium solver for aerosols (MESA), *J. Geophys. Res.*, *110*, D24203, doi:10.1029/2004JD005618.

Zaveri, R. A., R. C. Easter, J. D. Fast, and L. K. Peters (2008a), Model for simulating aerosol interactions and chemistry (MOSAIC), *J. Geophys. Res.*, *113*, D13204, doi:10.1029/2007JD008782.

Zaveri, R. A., et al. (2008b), Evolution of trace gases and aerosols in the Mexico City pollution outflow during a long range transport event, paper presented at AAAR 27th Annual Conference, Am. Assoc. for Aerosol Res., Orlando, Fla.

Zelenyuk, A., and D. Imre (2005), Single particle laser ablation time-of-flight mass spectrometer: An introduction to SPLAT, *Aerosol Sci. Technol.*, *39*, 554–568, doi:10.1080/027868291009242.

Zelenyuk, A., J. Yang, C. Song, R. A. Zaveri, and D. Imre (2008a), "Depth-profiling" and quantitative characterization of the size, composition, shape, density, and morphology of fine particles with SPLAT, a single-particle mass spectrometer, *J. Phys. Chem. A*, *112*, 669–677, doi:10.1021/jp077308y.

Zelenyuk, A., J. Yang, C. Song, R. A. Zaveri, and D. Imre (2008b), A new real-time method for determining particles' sphericity and density: Application to secondary organic aerosol formed by ozonolysis of α-pinene, *Environ. Sci. Technol.*, *42*, 8033–8038, doi:10.1021/es8013562.

Zelenyuk, A., D. Imre, J. H. Han, and S. Oatis (2008c), Simultaneous measurements of individual ambient particle size, composition, effective density, and hygroscopicity, *Anal. Chem.*, *80*, 1401–1407, doi:10.1021/ac701723v.

Zelenyuk, A., J. Yang, E. Choi, and D. Imre (2009), SPLAT II: An aircraft compatible, ultra-sensitive, high precision instrument for in-situ characterization of the size and composition of fine and ultrafine particles, *Aerosol Sci. Technol.*, *43*, 411–424, doi:10.1080/02786820802709243.

Zhang, Y., B. Pun, K. Vijayaraghavan, S.-Y. Wu, C. Seigneur, S. N. Pandis, M. Z. Jacobson, A. Nenes, and J. H. Seinfeld (2004), Development and application of the Model of Aerosol Dynamics, Reaction, Ionization, and Dissolution (MADRID), *J. Geophys. Res.*, *109*, D01202, doi:10.1029/2003JD003501.

J. C. Barnard, R. C. Easter, and R. A. Zaveri, Atmospheric Sciences and Global Change Division, Pacific Northwest National Laboratory, Richland, WA, USA. (rahul.zaveri@pnl.gov)

N. Riemer, Department of Atmospheric Sciences, University of Illinois at Urbana-Champaign, Urbana, IL, USA.

M. West, Department of Mechanical Science and Engineering, University of Illinois at Urbana-Champaign, Urbana, IL, USA.